1   **CONTEXT-DEPENDENT ENHANCER FUNCTION REVEALED BY**

2   **TARGETED INTER-TAD RELOCATION**

3

4   Christopher Chase Bolt[1,2,*], Lucille Lopez-Delisle[1], Aurélie Hintermann[2], Bénédicte Mascrez[2],

5   Antonella Rauseo[3], Guillaume Andrey[3] and Denis Duboule[1,2,4,*]

6
7
8

9   [1] School of Life Sciences, Ecole Polytechnique Fédérale de Lausanne (EPFL), 1015

10   Lausanne, Switzerland

11   [2] Department of Genetics and Evolution, Faculty of Sciences, University of Geneva, 30 quai

12   Ernest Ansermet, 1211, Geneva 4, Switzerland

13   [3] Department of Medical Genetics, Faculty of Medicine, University of Geneva, Rue Michel

14   Servet 1, 1211, Geneva 4, Switzerland

15   [4] Collège de France, 11 Place Marcelin Berthelot, 75231 Paris, France

16

17   Keywords: TADs, *Hox* genes, regulatory landscapes, enhancers, limb development

18

19   *Authors for correspondence:

20   denis.duboule@epfl.ch

21   christopher.bolt@unige.ch

22

23   **ABSTRACT**

24   The expression of genes with a key function during development is frequently controlled by

25   large regulatory landscapes containing multiple enhancer elements. These landscapes often

26   match Topologically Associating Domains (TADs) and sometimes integrate range of similar

27   enhancers, thus leading to TADs having a global regulatory specificity. To assess the relative

28   functional importance of enhancer sequences *versus* the regulatory domain they are included

29   in, we set out to transfer one particular enhancer sequence from its native domain into a TAD

30   with a closely related, yet different functional specificity. We used *Hoxd* genes and their

31   biphasic regulation during limb development as a paradigm, since they are first activated in

32   proximal limb cells by enhancers located in one TAD, which is then silenced at the time when

33   the neighboring TAD starts to activate its enhancers in distal limb cells. We introduced a strong

34   distal limb enhancer into the 'proximal limb TAD' and found that its new context strongly

35   suppresses its distal specificity, even though it continues to be bound by HOX13 transcription

36   factors, which normally are responsible for this activity. Using local genetic alterations and

37   chromatin conformation measurements, we see that the enhancer is capable of interacting with

38   target genes, with a pattern comparable to its adoptive neighborhood of enhancers. Its activity

39   in distal limb cells can be rescued only when a large portion of the surrounding environment is

40   removed. These results indicate that, at least in some cases, the functioning of enhancer

41   elements is subordinated to the local chromatin context, which can exert a dominant control

42   over its activity.

43
44

45 **INTRODUCTION**

46 Genes with important functions during vertebrate development are frequently multifunctional,
47 as illustrated by their pleiotropic loss-of-function phenotypes. This multi-functionality
48 generally results from the accumulation of tissue-specific enhancer sequences (Banerji et al.,
49 1981) around the gene. At highly pleiotropic loci, the collection of enhancers can be distributed
50 across large genomic intervals, which are referred to as regulatory landscapes (Bolt and
51 Duboule, 2020; Spitz et al., 2003). Such landscapes often correspond in linear size to
52 Topologically Associating Domains (TADs)(Dixon et al., 2012; Nora et al., 2012; Sexton et
53 al., 2012), defined as chromatin domains wherein the probability of DNA-to-DNA interactions
54 is higher than with neighboring domains. These collections of enhancers likely reflect an
55 evolutionary process whereby the emergence (or modification) of morphologies was
56 accompanied by novel regulatory sequences with the ability to be bound by tissue specific
57 factors, and hence alter the transcription of nearby target genes (Carroll et al., 2008).

58 This model, however, does not explicitly account for the potential influence of local genomic
59 context to modulate interactions between promoters and nascent enhancers, thus adding
60 another layer of complexity to our understanding of developmental gene regulation. For
61 instance, many developmental gene loci are initially decorated with the chromatin mark
62 H3K27me3 deposited by the Polycomb complex PRC2, before their activation (Bernstein et
63 al., 2005), possibly as a way to maintain silencing or limit transcription to very low levels.
64 These chromatin modifications disappear along with gene activation and are re-deposited once
65 the gene and its enhancers are progressively decommissioned, thus preventing inappropriate
66 transcription that may cause severe developmental problems (see Schuettengruber et al., 2017).
67 This indicates that enhancer or promoter function can be affected by their local chromatin
68 environments that may amplify both repressive or activating cues.

69 In the case of large regulatory landscapes containing many enhancers with similar tissue
70 specificity, the question arises as to how their activation and decommissioning are coordinated
71 and enforced over very large genomic intervals to overcome any contradictory inputs. Two
72 scenarios can be considered in this context. The first possibility is that each enhancer sequence
73 within the landscape independently responds to information delivered solely by the factors
74 bound to it in a sequence-specific manner. Such a mechanism would act entirely in *trans* and
75 its coordination would be ensured by the binding of multiple similar positive or negative
76 factors. In the second scenario, a higher level of regulation is imposed by the general
77 environment of the landscape, for example corresponding to a TAD-wide positive or negative
78 regulation, which would tend to dominate individual enhancer-specific controls in order to
79 minimize dangerous misexpression events.

80   To address this issue, we used the development of the vertebrate limb as a paradigm and, in

81   particular, the essential function of *Hox* genes in patterning and producing the main pieces of

82   tetrapod appendages (Zakany and Duboule, 2007). The emergence of the tetrapod limb

83   structure was a major evolutionary change that facilitated animal migration onto land. A key

84   step in this process was the acquisition of a fully developed distal part (hands and feet),

85   articulating with the more ancestral proximal parts of the limbs (e.g. the arm and the forearm).

86   During development, the distal piece requires the specific function of several key genes,

87   amongst which are *Hoxa13* and *Hoxd13*. While the absence of either gene function induces a

88   moderate phenotype in hands and feet (Dolle et al., 1993; Fromental-Ramain et al., 1996), the

89   double loss-of-function condition leads to the agenesis of these structures (Fromental-Ramain

90   et al., 1996) thus suggesting a critical function for these two genes both during the development

91   of distal limbs and its evolutionary emergence (see Woltering and Duboule, 2010). In this

92   context, the regulatory mechanisms at work to control expression of both genes in most distal

93   limb cells were carefully analyzed either for *Hoxa13* (Berlivet et al., 2013; Gentile et al., 2019),

94   or for *Hoxd13* (Montavon et al., 2011; Spitz et al., 2003), and found to be quite distinct from

95   one another.

96   In the case of *Hoxd* genes, the evolutionary co-option of *Hoxd13* into both the distal limbs and

97   the external genitals was accompanied by the emergence of a novel TAD (C-DOM) containing

98   multiple enhancers specific to either tissue or common to both (Acemel et al., 2016; Amândio

99   et al., 2020; Montavon et al., 2011; Woltering et al., 2014). This TAD is inactive until late in

100   development, when limb cells with a distal fate start to appear. In contrast, the expression of

101   other *Hoxd* genes (*Hoxd9*, *Hoxd10* and *Hoxd11*), which are all critical for the formation of

102   more proximal parts of the limb (Davis et al., 1995), are controlled by enhancers acting earlier

103   and located in the adjacent TAD (T-DOM)(Andrey et al., 2013). The *HoxD* cluster thus lies in

104   between these two TADs and contains several CTCF binding sites that create a boundary

105   between the two adjacent chromatin domains, insulating *Hoxd13* and *Hoxd12* from the rest of

106   the gene cluster (Rodriguez-Carballo et al., 2017). In the early stages of limb bud formation,

107   *Hoxd9*, *Hoxd10,* and *Hoxd11* are activated by the regulatory landscape located telomeric to the

108   cluster (T-DOM) leading to the patterning and growth of long bones of the arms and legs.

109   Subsequently, in a small portion of cells at the posterior and distal end of the early limb bud,

110   enhancers located in the centromeric regulatory landscape (C-DOM) are switched on, driving

111   expression of 5'-located *Hoxd* genes in the nascent hands and feet (Andrey et al., 2013).

112   The operations of these two TADs are mutually exclusive and as soon as C-DOM starts to

113   upregulate expression of *Hoxd13* in distal cells, enhancers within T-DOM are decommissioned

114   and a large part of this chromatin domain becomes decorated by H3K27me3 marks (Andrey et

115   al., 2013). This switch in TAD implementation involves the HOX13 proteins themselves since

116   their production in response to C-DOM enhancers participate in the repression of T-DOM

117   enhancers, likely through direct binding (Beccari et al., 2016; Sheth et al., 2016). In parallel,

118   HOX13 proteins positively regulate C-DOM enhancers, thus re-enforcing the functional switch

119   between the two TADs. In the absence of both HOXA13 and HOXD13, C-DOM is never

120   activated whereas T-DOM enhancers continue to function due to the absence of both

121   decommissioning and H3K27me3 coverage (Beccari et al., 2016). Therefore, in this context,

122   HOXD13 shows properties of both a transcriptional activator and a transcriptional repressor at

123   different times and in different chromatin environments.

124   At the time when *Hoxd13* becomes activated by distal limb (digit) enhancers, it is critical that

125   all proximal limb (forearm) enhancers are rapidly switched off, to prevent that the latter may

126   act on the former, a situation that was shown to be detrimental to limb morphology (Bolt et al.,

127   2021). This bimodal regulatory situation thus provides a paradigm to assay for the presence of

128   a 'context-dependent' repression of enhancer activity. Accordingly, we set out to introduce into

129   the proximal limb-specific T-DOM domain, the strongest distal enhancer normally working

130   within C-DOM to activate *Hoxd13* in digit cells, asking whether this distal limb regulatory

131   sequence would still be able to exert its function when relocated into a TAD where limb

132   enhancers are being repressed in distal cells. We report that this enhancer element, which is

133   functionally very penetrant when introduced at various random positions by non-targeted

134   transgenesis, loses most of its distal limb activity when recombined within T-DOM, even

135   though it continues to recruit the HOX13 factors, which are essential for its function in distal

136   limb cells. We further show that part of the distal limb activity is restored when large portions

137   of T-DOM are deleted *in-cis*. We conclude that the function of this enhancer is inhibited by an

138   *in cis* mechanism acting at the level of an entire chromatin domain, suggesting the existence,

139   in this particular case, of a level of regulation higher than that of the enhancer sequences

140   themselves.

141

142   **RESULTS**

143   **A distal-limb specific enhancer**

144   To evaluate how a tissue specific enhancer would behave when relocated into a

145   different chromatin and regulatory context, we searched for a candidate enhancer element that

146   would display the strongest possible specificity for developing distal limb cells at the *HoxD*

147   locus. We performed ATAC-seq in wild type E12.5 distal limb cells and compared the signals

148   with a previously reported H3K27ac ChIP-Seq dataset (Rodriguez-Carballo et al., 2017).

149   Because distal limb enhancers located at *Hox* loci were shown to colocalize with the binding

150   of HOX13 proteins as assayed in ChIP-seq experiments (Beccari et al., 2016; Sheth et al.,

151   2016), we used a CUT&RUN approach for both HOXA13 and HOXD13 (together referred to

152   as HOX13) to more precisely delineate enhancer elements controlled, at least in part, by these

153   transcription factors.

154   We identified a small element within a region previously described as Island II, one of

155   the islands of the C-DOM regulatory archipelago (Lonfat et al., 2014; Montavon et al., 2011).

156   This element was strongly bound by both transcription factors and accessible as judged by

157   ATAC-Seq, suggesting that it is an active enhancer element in distal limb cells and that it

158   controls the expression of the most posterior *Hoxd* genes there (Figure 1A). Upon closer

159   inspection, we found that the peak from CUT&RUN experiments matched precisely with the

160   peak observed in a previously reported E11.5 whole limb bud ChIP-Seq experiment for

161   HOXA13 and HOXD13 (Figure 1B, dark grey lines)(Sheth et al., 2016). It also matched a

162   small DNA fragment that is highly conserved across tetrapods but thus far absent from all

163   evaluated fish genomes including that of coelacanth (Figure S1A; dashed box). This element

164   had all of the hallmarks of an active distal limb enhancer controlled by HOX13 transcription

165   factors and hence we called it enhancer element II1.

166   To test if this short element indeed carries the enhancer activity reported for the large

167   versions of Island II (Figures 1B and S1A; green rectangles below), we cloned the sequence

168   (532bp, mm10 chr2:74075311-74075843) and constructed a reporter transgene where the

169   enhancer is located 5' to the *HBB* promoter and the *LacZ* gene (Figures 1B and S1A; II1 TgN),

170   and injected it into mouse pronuclei. Five founder animals were identified and then crossed

171   with wild types. Embryos were collected at E12.5 and stained for *LacZ*. Four of the founders

172   transmitted the transgene and produced strong distal limb specific staining (Figure 1C, top).

173   One of the four transmitting founders also had low staining levels in nearly the entire embryo

174   and another founder produced staining in the central nervous system. The four animals

175   transmitting limb staining displayed a pattern closely matching the expression domains of both

176   *Hoxd13* and *Hoxa13* (Figure 1C). The variation observed in staining in other tissues likely

177   resulted from different integration sites.

178   **Deletion of the II1 enhancer sequence**

179   The C-DOM regulatory landscape contains multiple enhancer elements that are

180   necessary to produce a robust activation of *Hoxd* genes in the distal limbs and genitals

181   (Amândio et al., 2020; Montavon et al., 2011) and our ATAC-Seq and CUT&RUN
182   experiments showed that element II1 is among the most strongly bound and accessible elements
183   throughout the C-DOM (Figure 1A). Because of this, we anticipated that it may make a
184   measurable contribution to the transcription of *Hoxd* genes in the distal limb. To determine
185   what effect this element contributes to the global regulatory activity of C-DOM, we used
186   CRISPR/Cas9 to delete the II1 enhancer element (Figures 1B and S1A; green rectangle Del
187   II1). Several founders were obtained and we produced embryos homozygous for this
188   (*HoxD*^{*DelII1*}) deletion. We collected embryos at E12.5, measured their levels of distal limb *Hoxd*
189   mRNAs by RT-qPCR and looked at the transcript distribution by *in situ* hybridization. Using
190   both approaches, we did not observe any significant change, neither in the level of *Hoxd* gene
191   transcription in the distal limbs of embryos missing the II1 enhancer (Figure S1B, C), nor in
192   the spatial distribution. While this result was somewhat surprising given how strong the signal
193   for H3K27ac, ATAC and HOX13 binding are, a similar lack of effect was observed when
194   single genital enhancers were deleted within this same C-DOM TAD. However, removing
195   several such enhancers had a cumulative effect thus demonstrating the regulatory resilience of
196   this regulatory landscape (Amândio et al., 2020).

Targeted insertion of a C-DOM enhancer into T-DOM

198   The T-DOM TAD contains multiple enhancers (Figure 2A, orange rectangles), which
199   activate *Hoxd* genes in proximal limb cells, and the deletion of T-DOM abolishes all *Hoxd*
200   gene transcripts from the proximal pieces of the growing limb buds (Andrey et al., 2013; Bolt
201   et al., 2021). In distal limb cells these elements are no longer at work and the entire T-DOM is
202   switched off at the same time as enhancers within C-DOM are activated, including the II1
203   element. HOX13 proteins bind throughout the T-DOM and are associated with the
204   decommissioning of the proximal limb enhancers. When HOX13 factors are not present the
205   decommissioning does not occur and the 'proximal' enhancers continue operating in distal cells
206   (Beccari et al., 2016). In fact, the T-DOM proximal enhancers CS39 and CS65 also operate in
207   distal cells when introduced randomly into the genome as transgenes (Beccari et al., 2016),
208   suggesting that the T-DOM environment represses the function of such sequences in distal
209   cells, and that this mechanism may involve the binding of HOX13 factors.

210   To further challenge this repressive effect and see whether it would dominate over the
211   strong distal specificity of an enhancer that normally operates in distal cells, we set up to
212   relocate a single copy of the enhancer II1 into T-DOM. We used the same transgenic construct
213   (Figure 1, II1 TgN) used to test the enhancer element by random insertion transgenesis (Figure
214   1C), but we attached homology arms to the 5' and 3' ends to target insertion to a region of T-

215   DOM in between - yet at a distance from - two strong CS39 and CS65 proximal limb enhancers

216   (Andrey et al., 2013; Beccari et al., 2016). This region was also selected because it had low

217   levels of the Polycomb Group histone H3 modification H3K27me3, such that H3K27me3 short

218   distance spreading (see Cheutin and Cavalli, 2019) would not directly impact the inserted

219   element. Fertilized eggs were injected with both the targeting construct and various CRISPR

220   components (Figure 2A, Table S1).

221   We identified two founder lines that carried the construct and produced *LacZ* staining.

222   The *HoxD*$^{II1\text{-}T\text{-}DOM\text{-}542}$ founder line ('allele 542') showed a strong *LacZ* staining in the proximal

223   limb (Figure 2B, black arrows), with very weak staining appearing in the distal limb from E12.5

224   onwards (Figure 2B, white arrows), limited to a small region of the forming digits. Since the

225   II1 transgene was located within T-DOM, which hosts multiple proximal limb enhancers, the

226   strong proximal limb activity likely resulted from the transgene behaving as an enhancer sensor

227   in these cells. The second line identified (*HoxD*$^{II1\text{-}T\text{-}DOM\text{-}320}$) produced a strikingly different

228   staining pattern (Figure 2C). At E10.5 both the II1 T-DOM 542 and II1 T-DOM 320 lines had

229   strong staining in the proximal limb, but not in the distal limb (Figure 2B, C; compare white

230   and black arrows). Then, at E11.5, while both lines continued to produce strong proximal limb

231   staining, the II1 320 line also had strong distal limb staining (Figure 2C, white arrows). By

232   E12.5 the staining pattern between the lines had almost completely diverged, with II1 T-DOM

233   542 showing strong proximal and very weak distal staining. In contrast the II1 T-DOM 320

234   line produced very strong distal staining but it was nearly absent in the proximal limb (Figure

235   2B, C).

236   To try to understand this difference and to confirm that the II1 transgene was inserted

237   at the expected position, we performed long-read sequencing with the Oxford Nanopore

238   MinION in conjunction with the nCATS protocol (Gilpatrick et al., 2020) to enrich for

239   sequencing reads covering the region around the insertion site (Figure S2A). In the 542 sample,

240   we were able to detect a sequencing read that extended the length of the transgene, both

241   homology arms, and several kilobases of the region that flanks the insertion (Figure S2B), thus

242   confirming that the 542 allele was a single copy transgene inserted correctly at the right site.

243   Because this enhancer was inserted into T-DOM (hereafter II1 T-DOM) producing the correct

244   allele, we used it for all subsequent experiments. We were not able to completely sequence the

245   II1 T-DOM 320 allele because it contained multiple tandem copies of the insertion, yet we

246   could reconstruct a putative genome based on unique overlapping reads which indicated that a

247   minimum of four copies of the transgene were inserted as a tandem array with multiple

248   orientations (Figure S2C).

249   From the analysis of these two alleles, we conclude that when inserted as a single copy
250 at the selected position within T-DOM, the distal limb enhancer activity of II1 was almost
251 entirely repressed and thus this sequence behaved there like any other native proximal limb
252 enhancers located in T-DOM (Andrey et al., 2013; Beccari et al., 2016). Since the heterologous
253 promoter trapped the activity of the surrounding proximal limb enhancers, the final pattern
254 appeared exactly as the reverse pattern for this enhancer when operating from C-DOM. This
255 positive response in proximal limb cells also acted as an internal control; the transgene was
256 capable of transcriptional activity, with a capacity for tissue specific expression. The repression
257 from the chromatin environment in distal cells was completely alleviated when the transgene
258 was present in multiple tandem copies, suggesting a potential micro-structure capable of
259 escaping the negative effect of the local TAD environment. The decreased expression of this
260 allele in proximal cells suggested that the array of transgenes was somehow insulated from
261 receiving the influence of T-DOM proximal enhancers.

262 **HOX13 transcription factors bind to II1 T-DOM in distal limb cells**

263   Despite the observed repression, when the II1 transgene was inserted into T-DOM as a
264 single copy, we scored a very low level of *LacZ* staining in E12.5 distal limb cells, detected
265 only at a late stage and appearing as defined spots in the digit mesenchyme, i.e., in cells that
266 do not reflect well the wild type expression pattern which is more widespread at this stage
267 (Figure 1C and 2B). Because the native II1 enhancer activity seems to be dependent on HOX13
268 proteins (Desanlis et al., 2020), we looked for both the accessibility of- and HOX13 binding to
269 the II1 element within the context of the inactive T-DOM in distal limb cells, to see if HOX13
270 factors could still access and bind the relocated enhancer sequence.

271   We first performed an ATAC-seq on embryos homozygous for the II1 T-DOM single-
272 copy insertion along with wild type controls. We mapped the reads on the mutant genome and
273 used a high mapping quality score (MAPQ30) to ensure that all reads observed on the coverage
274 tracks mapped uniquely to the native II1 element in C-DOM (II1 C-DOM) and the II1 transgene
275 recombined into T-DOM (II1 T-DOM). In wild type control samples, as expected, no ATAC
276 signal was observed over the native II1 C-DOM, neither in proximal limb bud cells, nor in
277 forebrain cells (Figure 3A left). In contrast, a strong ATAC signal appeared over the II1
278 element in distal limb cells (Figures 1B, 3A; DFL). In the II1 T-DOM transgene, there was a
279 weak signal observed over the *HBB* promoter element in forebrain and proximal limb cells, the
280 latter signal in proximal forelimb cells (PFL) likely reflecting the *LacZ* staining in response to
281 nearby proximal limb enhancers. In the distal forelimb samples (DFL), there was a further
282 increase in signal over the *HBB* promoter, and the accessible region extended over the II1

9

283   enhancer portion of the transgene. This signal over the II1 enhancer was nevertheless weaker
284   than that observed on the II1 element located in its native context (Figure 3A, ATAC DFL,
285   compare left and right).

286   The increased accessibility over the enhancer portion of the relocated II1 transgene in
287   T-DOM suggested that HOX13 transcription factor may still be able to bind. We assessed this
288   by performing CUT&RUN experiments using HOXA13 and HOXD13 antibodies on distal
289   limb cells from embryos homozygous for the II1 transgene in T-DOM and wild type controls.
290   To discriminate between reads from II1 in C-DOM or in T-DOM, only those reads containing
291   sequences uniquely mapping to sequences outside the II1 element itself were considered (see
292   methods). As expected, HOX13 proteins bound strongly to the native II1 element in C-DOM,
293   with a peak over the 3' end of the enhancer in controls (Figure 3A, left). At the analogous
294   position of the II1 transgene in T-DOM, we observed a similar peak for both HOXA13 and
295   HOXD13, indicating that HOX13 transcription factors were able to bind to the II1 enhancer
296   element when inserted into the T-DOM (Figure 3A, right). However, the presence of these
297   factors was not able to drive robust transcription of the nearby *LacZ* transgene in distal limb
298   bud cells.

299   To confirm that the HOX13 peaks detected in the II1 enhancer element indeed
300   corresponded to the presence of the expected HOX13 binding motif(s), we performed a motif
301   search analysis (Heinz et al., 2010) for our CUT&RUN samples and for a previously reported
302   dataset using ChIP-Seq (Sheth et al., 2016). In both datasets, we found motifs for HOX13
303   factors within the II1 element at four different positions. Three of these sites are closely
304   clustered at the 3' end of the enhancer element (Figure 3B, pink bars) and match the peak
305   summit for HOXA13 and HOXD13 in both the native II1 enhancer environment in C-DOM
306   and in the transgene in T-DOM (Figure 3A, grey columns). An additional motif was found
307   within the II1 region, but locates outside the peak region (Figure 3B, asterisk). The three
308   clustered motifs match previously reported HOX13 motifs (Desanlis et al., 2020; Sheth et al.,
309   2016) and their position in relation to the position of CUT&RUN reads suggested that these
310   sites are, in large part, responsible for the distal limb enhancer activity of the native II1 element
311   in C-DOM.

HOX13 binding sites are essential to II1 enhancer activity in distal limb buds

313   The presence of HOX13 factors bound to the II1 enhancer sequence when integrated
314   into T-DOM suggested that they may be responsible for the weak remaining *LacZ* staining in
315   some specific distal limb cells, even though this staining was distinct from the strong and

10

316   general accumulation scored with the randomly integrated transgene (II1 TgN, compare Figure

317   1C and 2B). Instead, it could be caused by some other factor(s) taking advantage of the pioneer

318   activity of HOX13 factors (Amândio et al., 2020; Desanlis et al., 2020). We verified this by

319   testing the necessity of these three HOX13 binding sites in the II1 enhancer recombined into

320   T-DOM. We implemented a CRISPR approach *in vivo* to delete the HOX13 binding sites in

321   the II1 T-DOM transgene, by using guides to delete either two or three of the HOX13 binding

322   sites (Figure 4A). Embryos hemizygous for the II1 enhancer in T-DOM were electroporated

323   with CRISPR guides and Cas9 protein and the embryos were collected at E12.5 and stained for

324   *LacZ*. Subsequently, the induced mutations were confirmed by Sanger sequencing (Table S2).

325   While the *LacZ* staining in proximal limb cells was not affected by these mutations, in all cases

326   where the binding sites were deleted, the remaining *LacZ* staining found in distal limb cells of

327   II1 T-DOM transgenic embryos was completely ablated even after overstaining the samples

328   (Figures 4B, Del TFBS and S4-1A).

329   Of note, in several F0 embryos, we observed very strong proximal and distal limb *LacZ*

330   expression (Figures 4B, S4-1B, Del C-T). When we sequenced the genomic DNA of these

331   embryos, we found that they all contained a large deletion extending from the native II1

332   enhancer element within C-DOM up to the II1 transgene within the T-DOM region

333   (approximately 1.2 Mb in length), due to the use of guide target sequences present in both

334   copies of the II1 sequence (scheme in Figure S4-1C). In these embryos, the HOX13 binding

335   sites are deleted and the *LacZ* transgene, formerly located within the T-DOM, was fused with

336   a portion of the C-DOM (Figure S4-1C). In such a configuration, it is very likely that the

337   enhancer remaining 5' to the II1 site in C-DOM (island I) was then able to act on the transgene

338   driving expression in the distal limb (Figures 4B and S4-1C), a regulatory influence obviously

339   not permitted in the presence of an integral native T-DOM. Expression in proximal cells was

340   controlled by those proximal enhancers located telomeric to the deletion breakpoint (Figure

341   2A, CS65 and PLEs).

342   As a control for the requirement of HOX13 factors for the function of the II1 enhancer

343   sequence, we generated two variants of the II1 TgN transgene construct lacking either two (Del

344   2x13) or three (Del 3x13) HOX13 binding sites (Figure 4C, Table S1). We then injected these

345   constructs into embryos to produce random integration events, and then stained for *LacZ*. In

346   nearly all cases, neither the Del 2x13, nor the Del 3x13 variants were able to produce distal

347   limb staining, when compared with the embryos containing the complete II1 enhancer sequence

348   (Figure 4D). There were two exceptions to this: in one Del 2x13 embryo, we observed a clear

349   distal limb staining although the proximal boundaries were very different than that seen in the

350   normal II1 transgene (Figure S4-2, Del 2x13, yellow asterisk) and, in one Del 3x13 embryo,

351 there was strong proximal limb staining and a portion of this staining extended into the

352 posterior portion of the distal limb (approximately digit 5), yet most of the distal limb staining

353 was absent (Figure S4-2, Del 3x13, yellow asterisk). In the remaining embryos carrying the

354 transgene, twenty-seven embryos with the Del 2x13 transgene and seventeen embryos with the

355 Del 3x13 transgene did not produce any distal limb staining (Figures 4D and S4-2).

356 As a final control experiment that integrates the two experiments above, we targeted

357 the insertion of two additional variants of the II1 transgene into the same position of T-DOM

358 as the II1 T-DOM 542 allele. In the first variant, we used the Del 3x13 transgene construction

359 used to test the need for the three HOX13 binding sites when integrated at random locations

360 throughout the genome (Figure 4C-D). When we stained embryos carrying this transgene, we

361 again observed very strong proximal limb staining that matched the 542 allele, indicating that

362 the transgene behaved as a T-DOM enhancer sensor in proximal limb cells (Figure S4-3A), but

363 there was no staining in the distal limb. In the second variant we completely removed the II1

364 enhancer element from the transgene and inserted into the T-DOM. In this construction the

365 *LacZ* staining pattern also produced strong proximal limb staining and no staining in the distal

366 limb (Figure S4-3B).

367 Altogether, these results indicate that even in the presence of bound HOX13 proteins,

368 which are normally the essential factors for its activation, the II1 enhancer sequence

369 recombined within T-DOM was unable to express its full potential. Indeed, only a weak

370 remnant of a transcriptional activity was scored in distal cells, at a late stage and low level,

371 even though the reporter system could work at high efficiency in proximal cells. This suggested

372 that, in distal limb cells, the surrounding chromatin context of T-DOM exerted a dominant

373 effect to repress the activity that this sequence normally displays when positioned within C-

374 DOM, even if the binding of HOX13 factors was still observed.

A TAD-driven repression of distal enhancers in proximal limb cells?

376 In order to challenge this negative in-*cis* effect, we used CRISPR to delete portions of

377 the T-DOM adjacent to the introduced enhancer transgene and then evaluated the effect of

378 these deletions on transcription of the transgenic *LacZ* construct. Fertilized eggs hemizygous

379 for the II1 T-DOM recombined enhancer allele were electroporated with CRISPR guides and

380 Cas9 protein (Table S1). Since the DNA sequences targeted by guides are present on both the

381 wild type and the II1 T-DOM alleles (Figure 5A, Table S1), we used genotyping PCR to screen

382 for embryos carrying the expected deletion and used changes in *LacZ* staining to associate the

383   deletion with the II1 T-DOM chromosome. As a control, we used littermate embryos that

384   contained the same deletion but on the wild type (non-transgenic) chromosome.

385   The first deletion extended from the 3' end of the *Mtx2* gene, up to, but not including,

386   the II1 enhancer element in the T-DOM (Figure 5A; Del *Mtx2*-II1-T-DOM). This deleted

387   region of T-DOM contains the CS39 and CS93 proximal limb enhancers (Andrey et al., 2013;

388   Yakushiji-Kaminatsu et al., 2018). In this deletion, we only scored a slight reduction in the

389   extent of the *LacZ* staining in proximal limb cells (Figure 5B, black arrows), likely due to the

390   removal of some proximal limb enhancers. In distal limb cells, there was a clear increase in the

391   *LacZ* staining throughout the distal limb mesenchyme spanning almost the entire digital plate,

392   as compared to the same deletion on the wild type chromosome (Figure 5B, compare left and

393   right, Figure S5A).

394   The second deletion extended from the 3' end of the *LacZ* transgene to the telomeric

395   end of the T-DOM regulatory landscape (Figure 5A, Del II1-T-DOM-*Hnrnpa3*). This portion

396   of T-DOM contains the CS65 and PLEs proximal limb enhancer elements (Andrey et al., 2013;

397   Bolt et al., 2021). In this deletion we observed a severe loss of *LacZ* staining in proximal limb

398   cells (Figure 5C, Figure S5B). In distal limb cells, there was a slight difference in the

399   distribution of *LacZ* positive cells, yet no obvious increase in staining when compared to the

400   control chromosome, unlike in the former deletion (Figure 5C, Figure S5B). These results

401   showed that staining could be recovered when the centromeric flanking piece of T-DOM was

402   removed and hence that this chromatin segment somehow exerted a robust repressive effect on

403   the II1 transgene in distal limb bud cells.

The II1 T-DOM transgene contacts the *HoxD* gene cluster

405   In distal limb bud cells at E12.5, strong chromatin contacts are detected between the II1

406   enhancer sequence (or a larger sequence including it) and the 'posterior' part of the *HoxD*

407   cluster. Along with other C-DOM cis-regulatory regions, the II1-*Hox* cluster interactions

408   collectively sustain activation of *Hoxd13* to *Hoxd11* in the digital plate (Montavon et al., 2011).

409   Because of this, we wondered how this enhancer sequence would behave when relocated within

410   the 3D chromatin space of the neighboring TAD. In other words, would it maintain its contacts

411   with these 'distal' limb genes (*Hoxd13* to *Hoxd11*), not establish any contacts with the cluster

412   at all, or would it adopt the interaction tropism of its new T-DOM neighborhood for the more

413   'proximal' limb genes (*Hoxd10*, *Hoxd9*, *Hoxd8*)? We performed Capture Hi-C (CHi-C) on

414   E12.5 proximal and distal forelimb cells micro-dissected either from wild type embryos, or

415   from embryos homozygous for the recombined II1 T-DOM transgene. The captured reads were

416   mapped onto the mutant genome excluding all reads that would ambiguously map to both the

417   II1 enhancer in C-DOM and in T-DOM, i.e., sequence reads that would not extend outside of

418   the enhancer itself and hence could not be uniquely assigned to either one of the two sites.

419   In both the proximal and distal forelimb datasets, strong contacts were established

420   between the II1 enhancer element within T-DOM and the *HoxD* gene cluster, as revealed by

421   the subtraction of the mutant contact signal from the wild type (Figure 6A, black arrows; Figure

422   S6A, black arrows). This gain of contacts between the recombined II1 enhancer and the *HoxD*

423   cluster in both proximal and distal cells, were the only noticeable change induced by the

424   presence of the transgene on the general chromatin configuration of the locus (Figure 6A). In

425   order to evaluate these new contacts in greater detail, we plotted pairwise heatmaps between

426   the *HoxD* cluster and II1 T-DOM, as well as H3K27me3, H3K27ac, and CTCF ChIP-seq

427   datasets (Rodriguez-Carballo et al., 2017; Yakushiji-Kaminatsui et al., 2018).

428   These alignments revealed clear differences between contacts in proximal and distal

429   cells, in both their relative strengths and localization. In proximal cells, the II1 enhancer and

430   the *HBB* promoter formed contacts mostly concentrated over the *Hoxd8* to *Hoxd10* region

431   (Figure 6B, grey dashed box). However, even at this 5kb resolution, we were not able to resolve

432   if the contacts were being mediated by the II1 transcription factor binding sites or the *HBB*

433   promoter, because both portions of the transgene are within the same *DpnII* restriction fragment

434   (Figure 6B, C). In distal limb bud cells, the contact dynamic was quite different. While the

435   fragment containing the II1 enhancer and the *HBB* promoter continued to form the strongest

436   contacts with the cluster, the region of highest contact had shifted from the 3' end of *Hoxd8* to

437   the 5' end, and the robust contacts detected around *Hoxd10* in proximal cells had nearly

438   disappeared (Figure 6C). Overall, the contacts were more evenly distributed over the region

439   extending from *Hoxd1* to *Hoxd9*, but they were excluded from the *Hoxd12* to *Hoxd13* region

440   (Figure 6C, grey dashed line).

441   The contacts between the II1 T-DOM transgene and the *HoxD* cluster changed between

442   proximal and distal limb bud cells, exactly matching the distribution of active *versus* inactive

443   chromatin in these two developmental contexts, respectively. In proximal limbs, the region of

444   enriched contacts corresponded to a depletion in H3K27me3 marks and an enrichment in

445   H3K27ac, which exactly matches the region of *HoxD* that is actively transcribed in proximal

446   limb cells (Andrey et al., 2013; Tarchini and Duboule, 2006). In distal limb cells, the contacts

447   became more evenly distributed and correlated with the presence of H3K27me3, stopping

448   abruptly within the H3K27ac-positive portion of *HoxD* cluster, before reaching *Hoxd13* and

449   *Hoxd12* (Figure 6C). Therefore, the II1 enhancer sequence, when recombined into T-DOM

14

450 behaved spatially like a strong T-DOM proximal limb enhancers (Figure S6A), even though it

451 had no intrinsic proximal limb specificity, as demonstrated by random transgenesis (Figure 1C,

452 Figure 4D). Regardless of the context and the developmental time, when positioned into T-

453 DOM, it never contacted the *Hoxd12* to *Hoxd13* region, which is the part of the cluster that this

454 enhancer sequence normally contacts with the highest affinity in distal limb bud cells, nor did

455 it influence in any way or in any cell type the chromatin structure that is normally found in T-

456 DOM.

457

DISCUSSION

459 The importance and status of enhancer sequences has evolved considerably since their

460 discovery (Banerji et al., 1981). Initially described as short non-coding sequences that can

461 increase the transcription rate of a target gene at a distance and regardless of orientation, they

462 are now known to modulate gene expression in many different ways (Schaffner, 2015).

463 Enhancers have a particular importance for genes with specialized expression patterns,

464 producing transcription in specific cell types and tissues, at precise times and quantities, either

465 during development or subsequently (Long et al., 2016). These sequences are thought to have

466 evolved along with the emergence of novel body structures, recruiting genes already functional

467 elsewhere, to accompany or trigger the formation of these novelties (Carroll et al., 2008). In

468 vertebrates, where multi-functionality is common for genes having important functions during

469 development, enhancers have accumulated in the vicinity of the transcription units forming

470 regulatory landscapes (Spitz et al., 2003) that sometimes extend over several megabases (see

471 (Bolt and Duboule, 2020). Within these landscapes, gene activation can be distributed across

472 multiple enhancers (Marinic et al., 2013; Montavon et al., 2011) often leading to functional

473 redundancy between them or to more complex interactions (Amândio et al., 2020; Osterwalder

474 et al., 2018). Alternatively, enhancer sequences can be grouped together in a more compact

475 manner, either to ensure a coordinated function, as exemplified by the *Globin* genes (Grosveld

476 et al., 2021; Liu et al., 2018; Oudelaar et al., 2021), or to maximize transcription in a given

477 cellular context such as the compact regulatory structure referred to as super enhancers (Blobel

478 et al., 2021; Hnisz et al., 2013).

479 Enhancers are often embedded into Topologically Associating Domains (TADs), which

480 are regions where certain DNA-DNA interactions are favored while adjacent regions are

481 excluded from the interaction space (Dixon et al., 2012; Nora et al., 2012; Sexton et al., 2012).

482 As illustrated at the *HoxD* locus, the genomic dimensions of TADs sometimes correspond to

483 the extents of regulatory landscapes (Andrey et al., 2013), with TADs providing boundaries to

15

484   the interaction space of enhancers within the three-dimensional organization of the genome.
485   Consequently, TADs have been considered to be permissive structures augmenting enhancer
486   and promoter interactions, while simultaneously providing borders that prevent enhancers from
487   interacting with elements outside the TAD, and hence to regulate genes in an inappropriate
488   manner (Lupianez et al., 2015, 2016). In this view, however, the enhancer sequence is
489   considered as a regulatory element that can explore and act within the nuclear space somewhat
490   freely unless TAD borders are present to frame its realm of action. Alternatively, there may be
491   some loci where the function of an enhancer sequence can be subordinated to the global
492   chromatin context of a given TAD thus introducing a level of regulatory control derived from
493   a large chromatin domain rather than by individual DNA sequences (Andrey et al., 2013;
494   Marinic et al., 2013; Rouco et al., 2021).

495   The transfer of enhancer II1 into T-DOM may illustrate such a case, where a potent and
496   highly penetrant enhancer sequence is inhibited precisely in those cells where it normally
497   functions, by placing it within a global environment that is not operational in these cells. In its
498   normal location among C-DOM enhancers, the II1 sequence is bound by HOX13 factors
499   (Beccari et al., 2016; Desanlis et al., 2020; Sheth et al., 2016), which are responsible for its
500   strong activation potential as demonstrated here by the deletion of these sites in the transgenic
501   context, which leads to the loss of *LacZ* staining in digit cells. When recombined into T-DOM,
502   the II1 enhancer is silenced yet it still recruits HOX13 factors and hence its silencing cannot
503   be attributed to the absence of the necessary activating factors. In fact, HOX13 factors are also
504   bound to T-DOM whenever this TAD becomes inactive in distal limb cells and covered by
505   H3K27me3 marks (Beccari et al., 2016), suggesting that the same factors may act in both a
506   positive and a negative manner in different chromatin contexts.

507   One potential explanation to this observation is that HOX13 factors may function with
508   more than one modality, depending on their context. On the one hand, these factors may bind
509   to and activate an enhancer-reporter transgene in a sequence-specific manner, as many
510   transcription factors do, leading to the pattern described herein and its absence in transgenes
511   lacking the binding sites. On the other hand, both HOXD13 and HOXA13 proteins contain a
512   large poly-alanine stretch (Bruneau et al., 2001), which may potentially drive the formation of
513   phase-separated globules by co-condensing with transcriptional co-activators/co-repressors, as
514   shown for these and other genes (Basu et al., 2020; Grosveld et al., 2021). It is thus possible
515   that, due to their high content in bound HOX13 proteins, which contain stretches of poly-
516   alanine (Bruneau et al., 2001), both C-DOM and T-DOM are used to form large transcription-
517   hub condensate (Grosveld et al., 2021)(Amândio et al., 2020), leading to a positive
518   transcriptional outcome for C-DOM in distal limb cells, and a negative outcome for T-DOM,

16

519 within the same cells, due to the inclusion of additional co-factors that are specific to each

520 domain (Karr et al., 2021). This latter explanatory framework would also account for why the

521 deletion of the enhancer II1 *in vivo* had essentially no detectable effect upon transcription of

522 target *Hoxd* genes in distal limbs, much like what was reported for C-DOM enhancers used for

523 external genitals (Amândio et al., 2020) as well as in other comparable instances (Osterwalder

524 et al., 2018). In both cases, removing a single component of the aggregate would not matter

525 too much, whereas removing several related enhancers would then have a measurable impact.

526 This situation contrasts those where a single enhancer is responsible for target gene

527 activation, the deletion of which usually seriously impairs the structure (see e.g. (Lettice et al.,

528 2003; Shapiro et al., 2004). However, the former mechanism would not preclude the capacity

529 for a single distal limb enhancer to trigger *LacZ* expression, as illustrated either by the weak

530 staining detected when II1 was relocated into T-DOM, or when a large deletion brought the

531 *LacZ* reporter close to Island 1, following the fusion between parts of C-DOM and T-DOM.

532 The II1 enhancer was selected because it is one of the strongest and most penetrant

533 distal limb cells enhancer reported thus far (Lonfat et al., 2014). Yet it was silenced when

534 introduced into T-DOM, along with several native T-DOM limb enhancers, which have a

535 strong proximal specificity when inside T-DOM, while they can work efficiently in distal cells

536 as well when randomly integrated as transgenes (Beccari et al., 2016). The repression of T-

537 DOM in distal limb cells is reflected by the presence of large arrays of H3K27me3 marks

538 (Andrey et al., 2013), and it is thus possible that the recombined II1 enhancer was included

539 into this negative chromatin domain. The analysis of the II1 T-DOM 320 line (Figure 2C)

540 suggests that this repression can be competed out by the presence of multiple copies of the

541 enhancer-reporter construct, perhaps due to the formation of a particular sub-structure escaping

542 the negative effect of T-DOM, or simply because of the accumulation of some transcription

543 factors. This line was nevertheless not analyzed further due to technical difficulties associated

544 with duplicated genomic sequences. We however conclude that special attention should be

545 given to copy number when interpreting results from transgenic experiments.

546 The negative effect of T-DOM over the II1 enhancer construct *in-cis* was further

547 suggested by our flanking deletions analyses. The (Del II1-T-DOM-*Hnrnpa3*) telomeric

548 deletion did not substantially change the weak distal staining of the transgene, yet it severely

549 reduced expression in the proximal domain, showing that the most potent proximal enhancers

550 were located in the deleted interval. In contrast, the (Del *Mtx2*-II1-T-DOM) centromeric

551 deletion consistently had the opposite effect, with only a slight reduction of the activity in the

552 proximal limb domain while distal expression was re-activated, thus mapping the main T-DOM

17

553 region carrying the repressive effect between the gene cluster and the integration site of the
554 enhancer-reporter construct. However, it was not assessed whether this reactivated distal *LacZ*
555 staining is due to the II1 enhancer itself or to the de-repression of other T-DOM enhancers,
556 which would then act on the *HBB* promoter due to the in-*cis* proximity.

557   Finally, the recombined II1 construct was able to specifically and rather strongly
558 contact the *HoxD* cluster, in both proximal (when T-DOM is active) and distal (when T-DOM
559 is inactive) limb bud cells. In these two instances, however, the contacts were distributed
560 differently. In proximal cells, contacts were established with the specific part of the cluster that
561 is heavily transcribed, following the behavior of other T-DOM located enhancers (Andrey et
562 al., 2013). In this case, these interactions were not directly driven by CTCF, for the integration
563 site was selected at a distance from such sites. The enhancer was likely included into a global
564 structure interacting with specific *Hoxd* promoters and possibly organized by CTCF sites
565 within both the gene cluster and T-DOM (Rodríguez-Carballo et al., 2020). In distal cells, the
566 interactions were less specific and likely reflected contacts between large H3K27me3
567 decorated chromatin segments (Noordermeer et al., 2011; Vieux-Rochas et al., 2015), as
568 suggested by the absence of contacts with those genes heavily transcribed in distal cells. There
569 again, the II1 enhancer behaved like its new neighboring proximal enhancers.

570 CONCLUSION

571   Altogether, we conclude that in distal limb bud cells, the necessary decommissioning
572 of all previously acting proximal enhancers is partly achieved -or secured- by a TAD-wide
573 silencing mechanism, as illustrated by the appearance of large domains of H3K27me3. This
574 mechanism is potent enough to prevent the expression of one of the strongest distal limb
575 enhancers, after its recombination within T-DOM. This silencing is partly alleviated when a
576 large piece of flanking chromatin is removed, suggesting the importance of neighboring
577 sequences within the TAD to achieve this effect. When this distal enhancer was introduced into
578 this 'proximal TAD', it behaved in all respects like its new neighbor proximal enhancers, thus
579 illustrating the potential of chromatin domains, in some cases, to impose another level of
580 coordinated regulation on top of enhancer sequence specificities.

581

582 **MATERIALS & METHODS**

583 **Animal work**

584 All experiments were approved and performed in compliance with the Swiss Law on Animal
585 Protection (LPA) under license numbers GE 81/14 and VD2306.2 (to D.D.). All animals were
586 kept in a continuous back cross with C57BL6 × CBA F1 hybrids. Sex of the embryos was not
587 considered in this study. Mice were housed at the University of Geneva Sciences III animal
588 colony with light cycle between 07:00 and 19:00 in the summer and 06:00 and 18:00 in winter,
589 with ambient temperatures maintained between 22 and 23 °C and 45 and 55% humidity, the air
590 was renewed 17 times per hour.

591 **Genotyping**

592 When samples were to be used directly for experiments, a rapid protocol was implemented:
593 Yolk sacs were collected and placed into 1.5 ml tubes containing Rapid Digestion Buffer
594 (10mM EDTA pH8.0 and 0.1mM NaOH) then placed in a thermomixer at 95º for 10 min with
595 shaking at 900 rpm. While the yolk sacs were incubating, the PCR master mix was prepared
596 with Z-Taq (Takara R006B)(see Table S1 for genotyping primers) and aliquoted into PCR
597 tubes. The tubes containing lysed yolk sacs were then placed on ice to cool briefly and quickly
598 centrifuged at high speed. The lysate (1ul) was placed into the reaction tubes and cycled 32X
599 (2s at 98º, 2s at 55º, 15s at 72º). 20ul of the PCR reaction was loaded onto a 1.5% agarose gel
600 and electrophoresis was run at 120V for 10 minutes. Alternatively, when samples could be kept
601 for some time, a more conventional genotyping protocol was applied; Tail Digestion Buffer
602 (10mM Tris pH8.0, 25mM EDTA pH8.0, 100mM NaCl, 0.5% SDS) was added to each yolk
603 sac or tail clipping at 250ul each along with 4ul Proteinase K at 20mg/ml (EuroBio
604 GEXPRK01-15) and incubated overnight at 55ºC. The samples were then incubated at 95º for
605 15 minutes to inactivate the Proteinase K and stored at -20ºC until ready for genotyping.
606 Genotyping primers (Table S1) were combined with Taq polymerase (Prospec ENZ-308) in
607 25ul reactions and cycled 2X with $T_a = 64$ºC and then cycled 32X with $T_a = 62$ºC.

608 *LacZ* **staining**

609 Embryos were collected in ice cold 1X PBS in a 12-well plate. They were then fixed for 5
610 minutes at room temperature in freshly prepared 4% PFA with gentle shaking on a rocker plate.
611 After fixing they were washed three times in washing solution (2mM MgCl2, 0.01% Sodium
612 Deoxycholate, 0.02% Nonidet P40, and 1X PBS) for 20 minutes each at room temperature on

19

613   a rocker plate. After approximately one hour of washing the wash solution was removed and

614   replaced with staining solution (5mM Potassium Ferricynide, 5mM Potassium Ferrocynide,

615   2mM MgCl2 hexahydrate, 0.01% Sodium Deoxycholate, 0.02% Nonidet P40, 1mg/ml X-Gal,

616   and 1X PBS). The plate was wrapped in aluminum foil and placed on a rocker plate over night

617   at room temperature. The following morning the staining solution was removed and the

618   embryos were washed three times in 1X PBS and then fixed in 4% PFA for long-term storage.

619   Images of embryos were collected with an Olympus DP74 camera mounted on an Olympus

620   MVX10 microscope using the Olympus cellSens Standard 2.1 software.

621   **Whole-mount *in situ* hybridization (WISH)**

622   Embryos were collected at E12.5 and processed following a previously reported WISH

623   procedure (Woltering et al., 2009). Briefly, embryos were fixed overnight in 4% PFA at 4ºC.

624   The following day they were washed and dehydrated through 3 washes in 100% methanol and

625   then stored at -20ºC until ready for processing. Each sample was prepared with Proteinase K

626   (EuroBio GEXPRK01-15) at 1:1000 for 10 min. Hybridizations were performed at 69ºC and

627   post-hybridization washes were performed at 65ºC. Staining was performed with BM-Purple

628   (Roche 11442074001). All WISH were performed at on at least three biological replicates.

629   Images of embryos were collected with an Olympus DP74 camera mounted on an Olympus

630   MVX10 microscope using the Olympus cellSens Standard 2.1 software.

631   **RT-qPCR**

632   Embryos were isolated from the uterus and placed into 1x DEPC-PBS on ice. The yolksacs

633   were collected for genotyping. The embryos were transferred into fresh 1x DEPC-PBS and the

634   distal limb portion was excised, placed into RNALater (ThermoFisher AM7020), and stored at

635   -80ºC until processing. Batches of samples were processed in parallel to collect RNA with

636   Qiagen RNEasy extraction kits (Qiagen 74034). After isolating total RNA, first strand cDNA

637   was produced with SuperScript III VILO (ThermoFischer 11754-050) using approximately

638   500ng of total RNA input. cDNA was amplified with Promega GoTaq 2x SYBR Mix and

639   quantified on a BioRad CFX96 Real Time System. Expression levels were determined by dCt

640   (GOI - Tbp) and normalized to one for each condition by dividing each dCT by the mean dCT

641   for each wild type set. Table S1 contains the primer sequences used for quantification. Box

642   plots for expression changes and two-tailed unequal variance t-tests were produced in

643   DataGraph 4.6.1.

644 **CUT&RUN**

645 Embryos were collected in ice-cold 1X PBS and yolk sacs were processed according to the
646 rapid genotyping protocol described above. Embryos with the correct genotype were
647 transferred to fresh PBS and dissected. The dissected tissue samples were transferred into 1X
648 PBS containing 10% FCS and then digested with collagenase (see ATAC-Seq protocol below).
649 For the HOXD13 and HOXA13 CUT&RUN, pools of cells from individual embryos were
650 processed. All samples were processed according to the CUT&RUN protocol (Skene et al.,
651 2018) using a final concentration of 0.02% digitonin (Apollo APOBID3301). Cells were
652 incubated with 0.5 ug/100ul of anti-HOXD13 antibody (Abcam ab19866), 0.5ug/100ul of anti-
653 HOXA13 (Abcam Ab106503) in Digitonin Wash Buffer at 4ºC. The pA-MNase was kindly
654 provided by the Henikoff lab (Batch #6) and added at 0.5ul/100ul in Digitonin Wash Buffer.
655 Cells were digested in Low Calcium Buffer and released for 30 minutes at 37ºC. Sequencing
656 libraries were prepared with KAPA HyperPrep reagents (07962347001) with 2.5ul of adaptors
657 at 0.3uM and ligated for 1 hour at 20ºC. The DNA was amplified for fourteen cycles. Post-
658 amplified DNA was cleaned and size selected using 1:1 ratio of DNA:Ampure SPRI beads
659 (A63881) followed by an additional 1:1 wash and size selection with HXB. HXB is equal parts
660 40% PEG8000 (Fisher FIBBP233) and 5M NaCl.

661 CUT and RUN libraries were sequenced paired-end on a HiSeq4000 sequencer and processed
662 as in (Bolt et al., 2021), mapped either on mm10 or on the Il1TDOM-542 mutant genome. The
663 E11.5 whole-forelimb HOXA13 and HOXD13 ChIP-Seq datasets (SRR3498934 of
664 GSM2151013 and SRR3498935 of GSM2151014) as well as E12.5 distal and proximal
665 forelimb H3K27Ac and CTCF ChIP-Seq datasets (SRR5855214 of GSM2713703,
666 SRR5855215 of GSM2713704, SRR5855220 of GSM2713707 and SRR5855221 of
667 GSM2713708) were processed similarly to what has been previously published (Beccari et al.,
668 2021). Adapter sequences and bad quality bases were removed with Cutadapt [Martin et al.
669 https://doi.org/10.14806/ej.17.1.200.] version 1.16 with options -a
670 GATCGGAAGAGCACACGTCTGAACTCCAGTCAC -A
671 GATCGGAAGAGCGTCGTGTAGGGAAAGAGTGTAGATCTCGGTGGTCGCCGTATC
672 ATT -q 30 -m 15 (−A being used only in PE data sets). Reads were mapped with bowtie
673 (Langmead and Salzberg, 2012) 2.4.1 with default parameters on mm10. Alignments with a
674 mapping quality below 30, as well as discordant pairs for PE datasets, were discarded with
675 samtools view version 1.8 (Li, 2011; Li et al., 2009). Coverage and peak calling were computed
676 by macs2 (Zhang et al., 2008) version 2.1.1.20160309 with options --bdg --call-summits --
677 gsize '1870000000', and -f BAMPE for PE. The HOX13 motifs where identified with

678   findMotifsGenome.pl from the Homer tool suite (Heinz et al., 2010) using the narrowPeak of

679   HOXA13 and HOXD13 ChIP as well as the third replicate of the HOXA13 and HOXD13 CUT

680   and RUN with the option -size 50. The best motif of each of these four datasets was used to

681   scan the sequence of the II1 enhancer. Four motifs were identified, for the three displayed in

682   Figure 2B, the logo of the motif giving the best score is shown.

683   **ATAC-Seq**

684   Samples used for ATAC-Seq were processed following the original protocol. Cells were

685   collected in 1X PBS on ice and yolk sacs were collected for each sample. Embryos were rapidly

686   genotyped (see above) and those with the correct genotype were transferred to fresh 1X PBS

687   and dissected. Tissue samples were transferred into 300ul 1X PBS containing 10% FCS on ice

688   until ready for processing. To each sample, 8ul of collagenase (at 50mg/ml, Sigma C9697) was

689   added and tubes were placed in a Thermomixer at 37° with shaking at 900rpm for

690   approximately 5 minutes or until the samples were completely disaggregated. The samples

691   were then placed into a centrifuge at 4°C and centrifuged at 500xg for 5 minutes. The

692   supernatant was removed and cells were gently resuspended in ice-cold 1X PBS. The cells in

693   each sample were counted with a Countess (ThermoFisher) using Trypan Blue and checked for

694   viability >90%. The volume needed to contain was 50,000 cells was determined and that

695   volume was transferred to a new tube and centrifuged at 4°C at 500xg for 5 minutes. The

696   supernatant was removed and the cell pellet was gently resuspended in lysis buffer then

697   immediately centrifuged at 500g for 10 minutes at 4°C. The lysis buffer was removed and the

698   cell pellet was gently resuspended in 50ul tagmentation mix (Nextera FC-121-1030) and then

699   incubated at 37° in a thermomixer at 300rpm for 30 minutes. The samples were then mixed

700   with Buffer QG from the Qiagen MinElute PCR Purification kit (28004) and processed

701   according to that protocol, and then eluted from the column in 11ul EB. Samples were stored

702   at -20°C until ready for library preparation. For library preparations, the samples were

703   amplified with Nextera Index Primers (FC-121-1011) using NEBNext High-Fidelity 2x PCR

704   Master Mix (M0541) and cycled 11 times. After PCR the reactions were cleaned first with the

705   Qiagen MinElute PCR Purification Kit and then with AMPure XP beads (A63881) at a ratio of

706   1.8:1.0 followed by elution with 15ul EB.

707   Adapter sequences and bad quality bases were removed with Cutadapt (Martin, 2011) version

708   1.16 with options -a CTGTCTCTTATACACATCTCCGAGCCCACGAGAC -A

709   CTGTCTCTTATACACATCTGACGCTGCCGACGA -q 30 -m 15. Reads were mapped with

710   bowtie (Langmead et al., 2009) 2.4.1 with parameters -I 0 -X 1000 --fr --dovetail --very-

711   sensitive on mm10 or on the II1TDOM-542 mutant genome. Alignments with a mapping

712   quality below 30, discordant pairs, and reads mapping to the mitochondria, were discarded with

713   bamtools version 2.4.0 [https://github.com/pezmaster31/bamtools]. PCR duplicates were

714   removed with Picard[http://broadinstitute.github.io/picard/index.html] version 2.18.2 before

715   the BAM to BED conversion with bedtools (Quinlan, 2014) version 2.30.0. Coverage and peak

716   calling were computed by macs2 (Zhang et al., 2008) version 2.1.1.20160309 with options --

717   format BED --gsize 1870000000 --call-summits --keep-dup all --bdg --nomodel --extsize 200

718   --shift -100.

719   **Capture Hi-C**

720   Samples used in the Capture Hi-C were identified by PCR screening embryos at E12.5 as

721   described above. Collagenase treated samples were cross-linked with 1% formaldehyde

722   (ThermoFisher 28908) for 10 minutes at room temperature and stored at -80º until further

723   processing. The SureSelectXT RNA probe design used for capturing DNA was done using the

724   SureDesign online tool by Agilent. Probes cover the region mm9 chr2:72240000-76840000

725   producing 2x coverage, with moderately stringent masking and balanced boosting. Capture and

726   Hi-C were performed as previously reported. Sequenced DNA fragments were processed as

727   previously reported but the mapping was performed on a mutant genome reconstructed from

728   minion and Sanger sequencing (see below). A custom R (www.r-project.org) script based on

729   the SeqinR package (Charif and Lobry, 2007) was used to construct a FASTA file for the

730   mutant chromosome 2 from the wild-type sequence and the exact position and sequence of

731   breakpoints.

732   Subtraction of matrices was performed with HiCExplorer (Ramirez et al., 2016; Wolff et al.,

733   2020, 2011) version 3.6. Heatmaps were plotted using a custom version (Lopez-Delisle et al.,

734   2021) of pyGenomeTracks (Ramírez et al., 2018) based on 3.6.

735   **II1 TgN Cloning and transgenesis**

736   The II1 enhancer sequence (mm10 chr2:74075305-74075850) was amplified from the fosmid

737   clone WI1-109P4 using primers 001 and 002 (Table S1). The 001 primer contains a *XhoI* site

738   and LoxP sequence followed by sequence to the II1 enhancer. The 002 primer contains at its

739   5' end a *HindIII* site. This PCR product was gel purified with Qiagen Gel Extraction Kit

740   (28704). The PCR fragment and the pSKlacZ reporter construct were digested with *XhoI* and

741   *HindIII* and ligated together with Promega 2X Rapid Ligation kit (C6711) to produce pSK-II1-

742   LoxP-*LacZ* construct. This vector (15ug) was cut with *XbaI* and *XhoI* to release the enhancer-

743   reporter construct. The digest was separated on a 0.7% agarose gel for 90 minutes. The 4190bp

744 fragment was excised from the gel and purified with Qiagen Gel Extraction Kit (28704) and

745 eluted in 30ul EB followed by phenol-chloroform extraction and ethanol precipitation and then

746 the pellet was dissolved in 30ul TE (5mM Tris pH7.5, 0.5mM EDTA pH8.0). DNA was

747 injected at 3ng/ul into pronuclei. Five founder animals were identified carrying the transgene

748 by PCR. Four male founders with the transgene were put into cross with wild type females and

749 embryos were collected at E12.5 to test for *LacZ* staining. All four male founder lines (*LacZ*/40,

750 41, 44, and 46) produced distal limb staining but *LacZ*/40 was chosen for amplification of the

751 breeding line due to high transmission of the transgene.

II1 T-DOM targeted insertion

753 The II1 TgN transgenic construct, outlined above, was used for the targeted insertion but

754 homology arms (HA) were attached (Left HA: mm10 chr2:75268556-75269591, Right HA:

755 mm10 chr2:75269617-75270665). The cloning vector was linearized with *KpnI*, separated on

756 a 0.7% agarose gel for 90 minutes at 90 volts, then the 9.0kb band was extracted and purified

757 two times with Qiagen Gel Extraction kit (28704). The DNA was quantified by Qubit dsDNA

758 and diluted to 5ng/ul with IDTE (11-05-01-05). Wildtype fertilized eggs were injected with the

759 construct and the supercoiled pX330 (Addgene #42230) expression vector containing the

760 sgRNA sequence (r4g9: mm10 chr2:75269597-75269616). Animals were genotyped (Table

761 S1) to identify founders, and then sequenced with minION (below).

minION Sequencing

763 Long-read sequencing was performed on the II1 T-DOM alleles (II1 T-DOM 320 and II1 T-

764 DOM 542) following the nCATS protocol with minor changes (Gilpatrick et al., 2020). Yolk

765 sacs were isolated from embryos containing the II1 T-DOM transgene and digested with Tail

766 Digestion Buffer (see above) and Proteinase K overnight at 55ºC with no shaking. The

767 following day the samples were incubated at 95ºC for 10 minutes to inactivate the Proteinase

768 K followed by ethanol precipitation and eluted in 200ul of 10mM Tris pH7.5. CRISPR guides

769 (Table S1) were designed in CHOPCHOP v3.0 (Labun et al., 2019) and synthesized as Alt-R

770 RNAs by IDT. CRISPR crRNAs were duplexed with tracrRNAs according to the IDT protocol

771 (Alt-R CRISPR-Cas9 System: In vitro cleavage of target DNA with ribonucleoprotein

772 complex, version 2.2). Two master mixes of guide RNAs and Cas9 protein (1081059) were

773 prepared (see Supplementary Figure 3 for sequence and cutting locations with the locus map),

774 containing either SCS-12 and SCS-13 or SCS-14. The gDNA (9ug) from the yolk sac was

775 dephosphorylated with NEB Quick CIP (M0510) for 10 minutes at 37ºC followed by 2 minutes

776   at 80ºC to inactivate the CIP. The gDNA was split into two equal pools and each pool was then

777   combined with the guideRNP master mixes to cut the gDNA for 30 minutes at 37ºC followed

778   by 5 minutes at 72ºC. The samples were then A-Tailed and AMX adaptors were ligated (Oxford

779   Nanopore SQK-LSK109). The reactions were size selected with 0.3X Ampure SPRI beads

780   (A63881) followed by two washes with Long Fragment Buffer and then eluted for 30 minutes

781   in 15ul EB. The DNA libraries were then prepared according to the Oxford Nanopore protocol

782   for sequencing on a minION (ENR_9084_v109_revP_04Dec2018). The sequencing ran for

783   approximately 24 hours and was stopped for processing after all nanopores were depleted.

784   Bases were called from the fast5 files using Guppy base-caller (Oxford Nanopore

785   Technologies) for CPU version 5.0.16+b9fcd7b. Reads were mapped on mm10 with minimap2

786   (Li, 2018) version 2.15 with parameter -ax map-ont. Only primary alignments were kept with

787   samtools view version 1.10 (Li, 2011; Li et al., 2009) and reads mapping to II1

788   (mm10:chr2:74073413-74076528) or to the insertion region (mm10:chr2:75262998-

789   75286118) were further analyzed. Read sequences were compared to the wild-type genome,

790   the expected mutant genome as well as the sequence of the cloning vector using a Perl script

791   as in (Schmidl et al., 2015) with the following modification: 20 bp of the MinION reads were

792   tested against the reference for 5 bp-sliding windows and only 20-mers completely identical to

793   unique 20-mers in the reference were kept. The output was then processed in R (www.r-

794   project.org) to display dot plots. The in-depth analysis of reads for allele 320 allowed to

795   propose a configuration that would match all reads containing in total four times the II1-*LacZ*

796   construct.

797   **Del II1 TFBS TgN cloning and transgenesis**

798   The enhancer constructs with mutations (Figure 4C) in the transcription factor binding sites

799   were constructed *in silico* and synthesized by TWIST Bioscience (San Francisco, CA). The

800   enhancer sequences are available in Table S1. The enhancer sequences were synthesized with

801   *BglII* and *AgeI* restriction sites at the 5' and 3' ends respectively. The mutant enhancer

802   sequences (Del 2x13 and Del 3x13) were restriction digested along with pSKlacZ and ligated

803   together with Promega 2X Rapid Ligation kit to produce pSK-II1Del2X13lacZ and pSK-

804   II1Del3X13lacZ. The enhancer-reporter fragments were released from the vector with *BglII*

805   and *XhoI* and purified as above. Pro-nuclear injections were performed by the transgenic

806   platform of the University of Geneva, medical school (CMU). Embryos were collected at

807   approximately E12.5 and stained for *LacZ*.

Deletions of transcription factor binding sites within T-DOM *in vivo*

Guide sequences were selected from the UCSC mm10 genome browser track CRISPR/Cas9 - NGG Targets. The crRNA Alt-R guides were synthesized by IDT. Males homozygous for the II1 T-DOM 542 allele were crossed with super-ovulated wild type females (BL6XCBA-F1) and fertilized eggs were collected. The embryos were electroporated with CRISPR guides (12ug of each guide) and TrueCut Cas9 v2 protein (Thermo Fisher A36497) with a NEPA21 (NEPA GENE Co. Ltd, Chiba, Japan) and then reimplanted into surrogate females. Embryos were collected at E12.5. Yolk sacs were digested and the II1:*HBB:LacZ* transgene was PCR amplified and Sanger sequenced to identify transgenic embryos containing the mutagenized enhancer element. Embryos that were mosaic for the mutation were not included in this analysis. The embryos were *LacZ* stained (see above) at 37º for 16 hours, washed in PBS and post-fixed, then stored in 70% ethanol for photographing.

Generation of Del *Mtx2*-II1-T-DOM and Del II1-T-DOM-*Hnrnpa3* alleles *in vivo*

The same methodology was used for this experiment as in the Del II1 T-DOM TFBS experiment above. The sequences for CRISPR guides used in this experiment are listed in Table S1. The embryos were genotyped for the presence of the deletion using primers in Table S1. Embryos with ambiguous genotyping results were not used in these results.

Targeted insertion of Del 3x13 and *HBB:LacZ* transgene in T-DOM of ESCs.

The two targeted insertions of control transgenes into T-DOM, genetic editing, and cellular culture were performed as previously reported (Figure S4-3) (Andrey and Spielmann, 2017; Kraft et al., 2015). The guide sequence (r4g9, Table S1) was cloned into pX459 vector from Addgene (#62988) and 8ug of the vector was used for mESC transfection. The pX459 vector was co-transfected with 4ug of the vector containing one of the two transgene cassettes. The two transgene cassettes (Del 3x13 and HBB:lacZ) contain the same vector backbone with the HBB promoter, lacZ gene, and SV40 polyA signal and homology arms used to target the r4 region of T-DOM (mm10 chr2:75269597-75269616). This is the same insertion site as the II1 T-DOM 542 and 320 alleles. The Del 3x13 contains the II1 enhancer element but with the three HOX13 binding sites removed (see Figure 4C, D). The HBB:lacZ transgene is the same but does not contain any portion of the II1 enhancer element so that it is strictly an enhancer sensor in the T-DOM. These constructs were co-transected into G4 mESCs obtained from the Nagy laboratory (George et al., 2007). After genotyping to confirm the insertion, the desired mESCs were thawed, seeded on male and female CD1 feeders and grown for 2 days before the

26

840 aggregation procedure. ESCs were then aggregated with tetraploid (c57bl6J x B6D2F1)
841 morula-stage embryos and let developed until blastula prior to transfer into CD1 foster females
842 by the transgenic mouse platform at the University of Geneva Medical School (Artus and
843 Hadjantonakis, 2011).
844

850 **ETHICS APPROVAL**

851 All experiments involving animals were performed in agreement with the Swiss Law on
852 Animal Protection (LPA), under license No. GE 81/14 (to DD).

853 **DATA AVAILABILITY**

854 All raw and processed datasets are available in the Gene Expression Omnibus (GEO)
855 repository under accession number GSE194114. All scripts necessary to reproduce figures
856 from raw data are available at https://github.com/lldelisle/scriptsForBoltEtAl2022
857

858 **COMPETING INTERESTS**

859 The authors declare that they have no competing interests.

AUTHOR CONTRIBUTIONS

C.C.B.: Designed and conducted experiments, analyzed datasets, formalized results and wrote the paper.

L.L-D. : Analyzed and evaluated the statistical significance of datasets. Wrote the paper.

B.M.: Produced and maintained all of the mouse lines.

A.H.: Performed the Del 2x13 and 3x13 experiment

A.R.: Performed the Del 3x13 T-DOM experiment

G.A.: Designed and performed the *HBB*:*LacZ* T-DOM experiment

D.D.: Designed experiments, transported mice, dissected some limb buds and wrote the paper.

880   **LEGENDS TO FIGURES**

881   **Figure 1**. **Identification of a distal limb bud specific enhancer**. **A**. ATAC-seq profile (top)
882   and binding profiles of both the HOXA13 (middle) and HOXD13 (bottom) transcription factors
883   by CUT&RUN, using E12.5 wildtype distal forelimb cells and covering the entire *HoxD* locus,
884   including the two flanking TADs C-DOM and T-DOM (mm10 chr2:73950000-75655000).
885   Green rectangles below are distal limb enhancers in C-DOM and orange rectangles are
886   proximal limb enhancers in T-DOM. The *Hoxd* gene cluster is indicated with a box at the center
887   and the *Lnpk* and *Mtx2* genes are indicated as rectangles with black borders. The *Hoxd13* gene
888   is on the centromeric end of the cluster and indicated by a purple box with a circle on the top,
889   whereas *Hoxd1* is telomeric and indicated by a square on top. The C-DOM Island II enhancer
890   (Montavon et al., 2011) is a green rectangle with a black border and its corresponding signals
891   are indicated by a dashed vertical rectangle. **B**. Magnification of the same tracks as above
892   centered around the Island II enhancer with, in addition, the H3K27ac ChIP-seq signal (top) in
893   E12.5 distal forelimbs (Rodriguez-Carballo et al., 2017). The profiles indicated by the dark
894   grey lines are from ChIP-seq using E11.5 whole limb buds (Sheth et al., 2016) for comparison
895   and are shown for comparison. Below the CUT&RUN profiles are the MACS2 peak summits
896   for the corresponding CUT&RUN samples. The green rectangles below indicate the regions
897   described as Island II in (Montavon et al., 2011) or in (Lonfat et al., 2014). The Del II1 shows
898   the region deleted in this work (Figure S1) and the II1 TgN is the transgene used panel in C.
899   **C.** *LacZ* staining pattern produced by the II1:*HBB:LacZ* (II1 TgN) enhancer reporter transgene
900   at E12.5, showing high specificity for distal limb cells (top). Below are whole-mount *in situ*
901   hybridizations for *Hoxa13* and *Hoxd13* in wild type E12. 5 forelimbs for comparison.

902

903   **Figure 2. Targeted recombination of the II1 reporter construct into T-DOM**. **A**. General
904   scheme of the *HoxD* locus with the two triangles on top showing the extents of both the C-
905   DOM (green) and T-DOM (orange) TADs. Various enhancers are shown either in green (distal
906   limbs) or yellow (proximal limbs) rectangles and the *HoxD* cluster is boxed. The large arrow
907   on top indicates the origin and new location of the island II enhancer transgene into T-DOM.
908   Below is a map of the II1:*HHB:LacZ* construct containing both left (L-HA) and right (R-HA)
909   homology arms, the II1 enhancer element and the *HBB* promoter with a *LacZ* reporter gene. **B**.
910   *B-galactosidase* staining time course and *LacZ* mRNAs (right panel) of the single-copy II1 T-
911   DOM 542 founder line. At E10.5 and 11.5, staining is very strong in the proximal limb (white
912   arrow) while absent in the distal portion (black arrow). By E12.5 weak staining appears in the
913   digit mesenchyme of the distal limb. The WISH for *LacZ* mRNA confirms that the distal limb
914   staining comes from transcription in distal limb cells rather than from stable *B-galactosidase*
915   activity. **C**. *B-galactosidase* staining of the multi-copy II1 T-DOM 320 founder line. Staining

916   is much stronger in this allele and similar to line 542 in E10.5 limb buds. However, by E11.5,

917   strong staining is gained in distal limb cells whereas it disappears from the proximal domain.

918

919   **Figure 3. HOX13 proteins bind to the II1 enhancer in T-DOM**. **A**. ATAC-Seq and

920   CUT&RUN reads mapped to the II1 enhancer sequence, either in its native environment within

921   C-DOM (left column; mm10 chr2:74074674-74076672), or after its targeted recombination

922   within T-DOM (line 542, right column; mm10 chr2:75268925-75270923). The green

923   rectangles below indicate the extent of the region used for the II1 enhancer element with, in

924   pink, the position of the three HOX13 binding sites. The II1 C-DOM element is not accessible

925   by ATAC-Seq in E12.5 forebrain (FB), nor in proximal forelimb cells (PFL) samples. At E12.5

926   it becomes highly accessible in distal forelimb cells (DFL) and is strongly bound by HOX13

927   proteins. The II1 element in T-DOM has low accessibility in the FB and PFL samples, even

928   though there is high transcription of the transgene in PFL. Similar to the II1 element in C-

929   DOM, the II1 enhancer in T-DOM is occupied by HOX13 proteins in distal limb cells. It also

930   shows an additional peak over the *HBB* promoter (orange arrow). This peak is likely a non-

931   specific signal resulting from promiscuous MNase activity used in the CUT&RUN technique.

932   In all samples but HOXD13 in the II1 T-DOM allele, experiments were performed in duplicate.

933   One replicate is plotted as a solid color and the other is shown as a superimposed black line. **B**.

934   On top is a schematic of the II1 enhancer element with the four HOX13 motif indicated as pink

935   bars. The pink bar with an asterisk indicates the motif position that is not in the HOX13 and

936   ATAC peak. At the bottom are the three HOX13 motifs identified by HOMER motif discovery

937   in the CUT&RUN experiments here and the E11.5 whole forelimb ChIP-seq (Sheth et al.,

938   2016).

939

940   **Figure 4. Deletions of HOX13 binding sites.** **A**. On top are shown the HOX13 motifs in the

941   II1 element, as extracted from the transcription factor binding (Figure 3B), with their positions

942   indicated below (light blue boxes with orientations). The dark blue boxes below the DNA

943   sequence indicate the positions and orientations of the CRISPR guides. Combinations of guides

944   were used to generate small deletions (g2 and g3 or g2 and g6). The yellow crosses indicate

945   the approximate cutting position of the Cas9. **B**. E12.5 F0 embryos stained for *LacZ*. The left

946   panel is a II1 T-DOM limb showing the staining pattern with the recombined II1 enhancer (no

947   CRISPR cutting), with weak staining in the distal limb, particularly in the digit mesenchyme.

948   The two central panels are representative embryos (n indicated in upper left corners) with the

949   indicated deletions (see Figure S4-1 for images of all embryos including these two #5083 and

950   #5146). Embryos carrying either the g2+g3 or g2+g6 deletions lost all staining in distal limb

951   cells. Several embryos showed strong distal limb staining (as shown in the right panel, see also

952   Figure S4-1B). They contained a large deletion that extends from the native II1 element in C-
953   DOM to the II1 transgenic element in T-DOM, due to the guide RNA sequences present at both
954   sites (scheme in Figure S4-1C). Deletions in all embryos were sequenced (Table S2). Embryos
955   with ambiguous sequencing results or mosaicism were not used. **C**. Sequence map of part of
956   the II1 enhancer elements used to generate randomly integrated transgenic embryos. The top
957   track is the wild type sequence around the three HOX13 binding sites for II1 used in control
958   embryos (II1 TgN ctrl). The Del 2x13 sequence lacks the two centromeric HOX13 binding
959   sites while the Del 3x13 sequence lacks all three HOX13 binding. **D**. On top are *LacZ* stained
960   E12.5 transgenic embryos and the table on the bottom reports the number of embryos that were
961   positive for the transgene by PCR (PCR+) followed but the number of embryos that stained in
962   the distal forelimb (DFL) as well as the embryos with no staining in the DFL (No DFL Stain).
963   The p-values are determined by Fisher's exact test. This indicates that the 2x13 and 3x13
964   deletions are likely to be responsible for the loss of distal limb staining in these embryos
965   compared with the II1 control embryos. The embryo on the left is a II1 control embryo
966   containing the wild type II1 sequence. The embryos in the center and right are representatives
967   of the staining (if any) obtained with the 2x13 and 3x13 constructs, with an absence of distal
968   limb staining. Pictures of all embryos generated in this experiment containing some *LacZ*
969   staining are in Figure S4-2, including the three shown here.

970

971   **Figure 5. Inhibition of distal enhancer activity by the T-DOM chromatin environment**.
972   **A.** Schematic of T-DOM with the *Hoxd* gene cluster on the left (purple boxes), *Hoxd1* with a
973   square and *Hoxd13* with a circle on top. The *Mtx2* gene is next to *Hoxd1* and *Hnrnpa3* gene is
974   the small white box with black border on the right of T-DOM. The position of the II1 transgene
975   insertion into T-DOM is indicated by a green rectangle with black border (mm10
976   chr2:75269597-75269616). Orange rectangles are known proximal limb enhancers. The two
977   regions deleted by CRISPR are indicated above the genomic map (Del *Mtx2*-II1-T-DOM and
978   Del II1-T-DOM-*Hnrnpa3*). **B.** Effect of deleting the centromeric portion of T-DOM (Del *Mtx2*-
979   II1-T-DOM) on *LacZ* staining, with a light loss of staining in the proximal domain (black
980   arrows) and a gain in the distal domain (see also Figure S5A). **C**. Effect of deleting the
981   telomeric portion of T-DOM (Del II1-T-DOM-*Hnrnpa3*) on *LacZ* staining, with an almost
982   complete loss of staining in the proximal domain (arrows) and no substantial impact on the
983   distal domain (see also Figure S5B). The embryos shown here are also displayed in Figure S5
984   to show the complete series of stained embryos.

985

986   **Figure 6. The II1 enhancer in T-DOM contacts the *Hoxd* gene cluster. A.** Capture Hi-C
987   maps at 5kb bin resolution over the entire *HoxD* locus (mm10 chr2:73950000-75655000),

988   displayed as the subtraction of wild type signal (blue) from the II1 T-DOM 542 allele signal
989   (red). The II1 enhancer T-DOM insertion site (arrow on the green rectangle at the bottom)
990   produces increased contacts with the *Hoxd* gene cluster (black arrow pointing to the red bins).
991   The contacts are established in both proximal forelimb (PFL) and distal forelimb (DFL) cells.
992   **B.** Contacts between the *Hoxd* gene cluster (x-axis, genes are indicated below) and the region
993   covering the II1 T-DOM reporter transgene (y-axis). The II1 T-DOM construct is schematized
994   on the y-axis for clarity, with a solid black line indicating the boundary between bins. The II1
995   enhancer is shown in green, the *HBB* promoter is black, and the *LacZ* gene is in grey. The
996   panels below are the H3K27ac, H3K27me3 (from (Yakushiji-Kaminatsui et al., 2018) and
997   bound CTCF (from (Rodriguez-Carballo et al., 2017) from wild type PFL cells, aligned with
998   the interaction matrix above. The strongest contacts are between the II1 T-DOM reporter
999   transgene and the region around *Hoxd8* and *Hoxd10*, matching genes transcribed in proximal
1000   limb cells, indicated by a grey dashed box. **C.** Same as in B but using distal forelimb cells
1001   (DFL). The II1 T-DOM insert establishes more diffuse contacts, extending from *Hoxd1* to
1002   *Hoxd11* and stopping abruptly before those genes highly expressed in distal cells (*Hoxd12*,
1003   *Hoxd13*).

1004

1005

1006   **LEGENDS TO SUPPLEMENTARY FIGURES**

1007   **Supplementary Figure S1. Deletion of the II1 enhancer does not alter *Hoxd* gene**
1008   **expression in the distal limb bud cells**. **A**. Magnified representation of the Island II1 enhancer
1009   element (mm10 chr2:74072912-74077028, (Montavon et al., 2011). HOXA13 (top) and
1010   HOXD13 (bottom) E12.5 CUT&RUN profiles are indicated by light or dark blue, whereas
1011   HOXA13 and HOXD13 E11.5 forelimb ChIP-seq profiles (Sheth et al., 2016) are shown as
1012   dark grey lines super-imposed for comparison. The DNA sequence conservation track MultiZ
1013   from UCSC (mm10) is shown below, with the most conserved region indicated with a bracket.
1014   **B**. RTqPCR for multiple *Hoxd* genes using distal forelimb bud cells from E12.5 wild type and
1015   homozygous Del II1 mutant specimen. P-value is indicated above, no significant difference in
1016   expression was detected for any *Hoxd* genes in the absence of the II1 enhancer (two-tailed
1017   unequal variance t-test). **C**. Whole-mount *in situ* hybridizations for *Hoxd13* and *Hoxd11* in
1018   embryos homozygous for the II1 enhancer deletion also show no change in their expression
1019   domains when this enhancer is deleted from C-DOM.

1020   **Supplementary Figure S2**. **Long-read sequencing of the genomic structure after targeted**
1021   **insertion.** **A**. Map of the T-DOM after homologous recombination of the II1:*HBB:LacZ*
1022   enhancer-reporter transgene, indicating the location of CRISPR guides used in the nCATS

1023   protocol for enrichment of sequencing reads (Gilpatrick et al., 2020). The red crosses indicate

1024   the location of the CRISPR cutting guide (see Supplementary Table S1). Two guides were used

1025   outside the II1 transgene (SCS12 and 13) and one guide within the II1 transgene (SCS14).

1026   Below the map of the CRISPR cutting position is a map of the transgene construct. The colors

1027   indicated for different portions of the construct match to the sequencing alignments below. **B**.

1028   Dotplot maps of sequencing reads recovered from the II1 T-DOM 542 allele and showing a

1029   clear one-copy recombination at the expected site. The x-axis is the position along the mutant

1030   II1 T-DOM 542 chromosome and the values on the y-axis represent the base pair position of

1031   the transgene. Each circle represents a 20bp alignment (see methods) so multiple adjacent 20bp

1032   matching reads appear as a line. The best matching read is drawn in black, while shorter reads

1033   are drawn in grey. **C**. Dotplot maps of five sequencing reads recovered from the II1 T-DOM

1034   320 allele, showing insertion of multiple copies.

1035   **Supplementary Figure S4-1**. **Photos of all embryos containing the deletions of the HOX13**

1036   **binding sites present in the II1 enhancer-reporter construct targeted into T-DOM**.

1037   Individual embryos are numbered. Embryos #5083 and #5146 are already shown in Figure 4B,

1038   but are reproduced here for easier comparison. The g2 + g3 and g2 + g6 deletions removed

1039   only binding sites within the II1 enhancer. **B**. Staining of embryos containing the Del C-T

1040   deletion. These embryos are positive in both proximal and distal limb bud cells. Embryo #5150

1041   is already shown in Figure 4B but is added here for comparison. **C**. Schematic of the Del C-T

1042   deletion. The Del C-T created a large deletion fusing parts of T-DOM and C-DOM due to the

1043   presence of the sequence targeted by the guides RNAs on both native (C-DOM) and transgenic

1044   (T-DOM). After deletion, the II1 *LacZ* reporter transgene is flanked by a centromeric distal

1045   limb enhancer (green) and several telomeric proximal enhancers (CS65, PLEs, orange), thus

1046   accounting for its expression in both limb domains.

1047   **Supplementary Figure S4-2**. **Photos of randomly integrated transgenic embryos stained**

1048   **for *LacZ* expression when HOX13 binding sites were deleted from the II1 enhancer**. The

1049   left two columns (II1 TgN ctrl) are control embryos containing the entire II1 enhancer

1050   sequence. The two columns in the center (Del 2x13) show stained embryos containing the II1

1051   enhancer element lacking the two centromeric HOX13 binding sites (see Figure 4A, C). The

1052   two columns in the right (Del 3x13) show stained embryos lacking all three HOX13 binding

1053   sites. The orange arrows indicated the location of *LacZ* staining when it is not detected in the

1054   distal limb buds. The unique embryo ID is shown at the bottom of each picture. The three

1055   embryos # cb09 04, cb17 05 and cb15 01 are those also displayed in Figure 4D. There are

1056   reproduced here for easier comparison. The two outlier embryos showing staining in distal limb

1057   cells are shown with a yellow asterisk.

1058 **Supplementary Figure S4-3.** *LacZ* **staining pattern in control transgenes inserted into T-**
1059 **DOM. A**. The *LacZ* staining in a control embryo containing the Del 3x13 variant of the II1
1060 enhancer. This variant contains the same targeting construct as the II1 T-DOM 542 allele, but
1061 the II1 enhancer has been replaced with the same variant used to produce the randomly
1062 integrated Del 3x13 (Figure 4D). The staining is very strong in the proximal limb and
1063 completely absent in the distal limb. This corroborates the observation from Figure 4, that the
1064 three HOX13 binding sites in II1 are necessary for the distal limb staining either as a randomly
1065 integrated transgene or a targeted insertion transgene in the T-DOM. **B**. The *LacZ* staining in
1066 a control embryo that does not contain the II1 enhancer element. This transgene contains the
1067 same targeting construct as the II1 T-DOM 542, but without the enhancer. The staining is very
1068 strong in the proximal limb and completely absent in the distal limb.

1069 **Supplementary Figure S5**. **Photos of all embryos carrying large deletions flanking the**
1070 **insertion of the of II1 enhancer-reporter construct within T-DOM** (see Figure 5B, C). All
1071 embryos were genotyped for the expected deletion. All embryos with the expected deletions
1072 are represented here unless they produce ambiguous PCR results or were mosaic for the
1073 deletion. The embryos #4470, 5023, 4492, 4491 from Figure 5 are reproduced here for easier
1074 comparison.

1075 **Supplementary Figure S6**. **Capture Hi-C maps**. Capture Hi-C maps covering the entire
1076 *HoxD* locus for wild type (wt) and the II1 enhancer recombined within T-DOM (II1 T-DOM),
1077 using both proximal (PFL) and distal (DFL) forelimb cells samples (mm10 chr2:73950000-
1078 75655000). The new contacts formed between the II1 enhancer-promoter sequence and the
1079 *Hoxd* gene cluster are indicated by the black arrow. The contacts were scored in both PFL and
1080 DFL cells, yet with a difference in resolution, being more diffuse in the DFL cells (see Figure
1081 6). The black arrows below points to the location of the II1 enhancer within C-DOM and the
1082 transgene integration site within T-DOM. The *HoxD* cluster position is indicated at the center.
1083 The *Hoxd13* gene is indicated by a purple pin with a circle and the *Hoxd1* is indicated with a
1084 square.

1085

1086 **REFERENCES**

1087 Acemel, R.D., Tena, J.J., Irastorza-Azcarate, I., Marletaz, F., Gomez-Marin, C., de la Calle-
1088 Mustienes, E., Bertrand, S., Diaz, S.G., Aldea, D., Aury, J.M., et al. (2016). A single three-
1089 dimensional chromatin compartment in amphioxus indicates a stepwise evolution of
1090 vertebrate Hox bimodal regulation. Nat Genet *48*, 336–341.

1091   Amândio, A.R., Lopez-Delisle, L., Bolt, C.C., Mascrez, B., and Duboule, D. (2020). A

1092   complex regulatory landscape involved in the development of mammalian external genitals.

1093   ELife *9*, e52962.

1094   Andrey, G., and Spielmann, M. (2017). CRISPR/Cas9 Genome Editing in Embryonic Stem

1095   Cells. Methods Mol. Biol. Clifton NJ *1468*, 221–234.

1096   Andrey, G., Montavon, T., Mascrez, B., Gonzalez, F., Noordermeer, D., Leleu, M., Trono,

1097   D., Spitz, F., and Duboule, D. (2013). A switch between topological domains underlies HoxD

1098   genes collinearity in mouse limbs. Science *340*, 1234167.

1099   Artus, J., and Hadjantonakis, A.-K. (2011). Generation of Chimeras by Aggregation of

1100   Embryonic Stem Cells with Diploid or Tetraploid Mouse Embryos. In Transgenic Mouse

1101   Methods and Protocols, M.H. Hofker, and J. van Deursen, eds. (Totowa, NJ: Humana Press),

1102   pp. 37–56.

1103   Banerji, J., Rusconi, S., and Schaffner, W. (1981). Expression of a beta-globin gene is

1104   enhanced by remote SV40 DNA sequences. Cell *27*, 299–308.

1105   Basu, S., Mackowiak, S.D., Niskanen, H., Knezevic, D., Asimi, V., Grosswendt, S.,

1106   Geertsema, H., Ali, S., Jerković, I., Ewers, H., et al. (2020). Unblending of Transcriptional

1107   Condensates in Human Repeat Expansion Disease. Cell *181*, 1062-1079.e30.

1108   Beccari, L., Yakushiji-Kaminatsui, N., Woltering, J.M., Necsulea, A., Lonfat, N., Rodriguez-

1109   Carballo, E., Mascrez, B., Yamamoto, S., Kuroiwa, A., and Duboule, D. (2016). A role for

1110   HOX13 proteins in the regulatory switch between TADs at the HoxD locus. Genes Dev *30*,

1111   1172–1186.

1112   Beccari, L., Jaquier, G., Lopez-Delisle, L., Rodriguez-Carballo, E., Mascrez, B., Gitto, S.,

1113   Woltering, J., and Duboule, D. (2021). Dbx2 regulation in limbs suggests interTAD sharing

1114   of enhancers. Dev. Dyn. Off. Publ. Am. Assoc. Anat. *250*, 1280–1299.

1115   Berlivet, S., Paquette, D., Dumouchel, A., Langlais, D., Dostie, J., and Kmita, M. (2013).

1116   Clustering of tissue-specific sub-TADs accompanies the regulation of HoxA genes in

1117   developing limbs. PLoS Genet *9*, e1004018.

1118   Bernstein, B.E., Kamal, M., Lindblad-Toh, K., Bekiranov, S., Bailey, D.K., Huebert, D.J.,

1119   McMahon, S., Karlsson, E.K., Kulbokas, E.J., Gingeras, T.R., et al. (2005). Genomic maps

1120   and comparative analysis of histone modifications in human and mouse. Cell *120*, 169–181.

1121   Bolt, C.C., and Duboule, D. (2020). The regulatory landscapes of developmental genes.

1122   Development *147*, dev171736.

1123   Bolt, C.C., Lopez-Delisle, L., Mascrez, B., and Duboule, D. (2021). Mesomelic dysplasias

1124   associated with the HOXD locus are caused by regulatory reallocations. Nat. Commun. *12*,

1125   5013.

1126   Bruneau, S., Johnson, K.R., Yamamoto, M., Kuroiwa, A., and Duboule, D. (2001). The

1127   mouse Hoxd13(spdh) mutation, a polyalanine expansion similar to human type II

1128   synpolydactyly (SPD), disrupts the function but not the expression of other Hoxd genes. Dev.

1129   Biol. *237*, 345–353.

1130   Buenrostro, J.D., Giresi, P.G., Zaba, L.C., Chang, H.Y., and Greenleaf, W.J. (2013).

1131   Transposition of native chromatin for fast and sensitive epigenomic profiling of open

1132   chromatin, DNA-binding proteins and nucleosome position. Nat. Methods *10*, 1213–1218.

1133   Carroll, S.B., Prud'homme, B., and Gompel, N. (2008). Regulating evolution. Sci Am *298*,

1134   60–67.

1135   Charif, D., and Lobry, J.R. (2007). SeqinR 1.0-2: A Contributed Package to the R Project for

1136   Statistical Computing Devoted to Biological Sequences Retrieval and Analysis. In Structural

1137   Approaches to Sequence Evolution: Molecules, Networks, Populations., U. Bastolla, M.

1138   Porto, H.E. Roman, and M. Vendruscolo, eds. (New York, USA: Springer Verlag), pp. 207–

1139   232.

1140   Cheutin, T., and Cavalli, G. (2019). The multiscale effects of polycomb mechanisms on 3D

1141   chromatin folding. Crit. Rev. Biochem. Mol. Biol. *54*, 399–417.

1142   Davis, A.P., Witte, D.P., Hsieh-Li, H.M., Potter, S.S., and Capecchi, M.R. (1995). Absence

1143   of radius and ulna in mice lacking hoxa-11 and hoxd-11. Nature *375*, 791–795.

1144   Desanlis, I., Kherdjemil, Y., Mayran, A., Bouklouch, Y., Gentile, C., Sheth, R., Zeller, R.,

1145   Drouin, J., and Kmita, M. (2020). HOX13-dependent chromatin accessibility underlies the

1146   transition towards the digit development program. Nat. Commun. *11*, 2491.

1147   Dixon, J.R., Selvaraj, S., Yue, F., Kim, A., Li, Y., Shen, Y., Hu, M., Liu, J.S., and Ren, B.

1148   (2012). Topological domains in mammalian genomes identified by analysis of chromatin

1149   interactions. Nature *485*, 376–380.

1150   Dolle, P., Dierich, A., LeMeur, M., Schimmang, T., Schuhbaur, B., Chambon, P., and

1151   Duboule, D. (1993). Disruption of the Hoxd-13 gene induces localized heterochrony leading

1152   to mice with neotenic limbs. Cell *75*, 431–441.

1153   Fromental-Ramain, C., Warot, X., Messadecq, N., LeMeur, M., Dolle, P., and Chambon, P.

1154   (1996). Hoxa-13 and Hoxd-13 play a crucial role in the patterning of the limb autopod.

1155   Development *122*, 2997–3011.

1156   Gentile, C., Berlivet, S., Mayran, A., Paquette, D., Guerard-Millet, F., Bajon, E., Dostie, J.,

1157   and Kmita, M. (2019). PRC2-Associated Chromatin Contacts in the Developing Limb Reveal

1158   a Possible Mechanism for the Atypical Role of PRC2 in HoxA Gene Expression. Dev. Cell

1159   *50*, 184-196.e4.

1160   George, S.H.L., Gertsenstein, M., Vintersten, K., Korets-Smith, E., Murphy, J., Stevens,

1161   M.E., Haigh, J.J., and Nagy, A. (2007). Developmental and adult phenotyping directly from

1162   mutant embryonic stem cells. Proc. Natl. Acad. Sci. U. S. A. *104*, 4455–4460.

36

1163 Gilpatrick, T., Lee, I., Graham, J.E., Raimondeau, E., Bowen, R., Heron, A., Downs, B.,

1164 Sukumar, S., Sedlazeck, F.J., and Timp, W. (2020). Targeted nanopore sequencing with

1165 Cas9-guided adapter ligation. Nat. Biotechnol. *38*, 433–438.

1166 Grosveld, F., van Staalduinen, J., and Stadhouders, R. (2021). Transcriptional Regulation by

1167 (Super)Enhancers: From Discovery to Mechanisms. Annu. Rev. Genomics Hum. Genet. *22*,

1168 127–146.

1169 Heinz, S., Benner, C., Spann, N., Bertolino, E., Lin, Y.C., Laslo, P., Cheng, J.X., Murre, C.,

1170 Singh, H., and Glass, C.K. (2010). Simple combinations of lineage-determining transcription

1171 factors prime cis-regulatory elements required for macrophage and B cell identities. Mol. Cell

1172 *38*, 576–589.

1173 Karr, J.P., Ferrie, J.J., Tjian, R., and Darzacq, X. (2021). The transcription factor activity

1174 gradient (TAG) model: contemplating a contact-independent mechanism for enhancer-

1175 promoter communication. Genes Dev.

1176 Kraft, K., Geuer, S., Will, A.J., Chan, W.L., Paliou, C., Borschiwer, M., Harabula, I., Wittler,

1177 L., Franke, M., Ibrahim, D.M., et al. (2015). Deletions, Inversions, Duplications: Engineering

1178 of Structural Variants using CRISPR/Cas in Mice. Cell Rep. *10*, 833–839.

1179 Labun, K., Montague, T.G., Krause, M., Torres Cleuren, Y.N., Tjeldnes, H., and Valen, E.

1180 (2019). CHOPCHOP v3: expanding the CRISPR web toolbox beyond genome editing.

1181 Nucleic Acids Res. *47*, W171–W174.

1182 Langmead, B., and Salzberg, S.L. (2012). Fast gapped-read alignment with Bowtie 2. Nat

1183 Methods *9*, 357–359.

1184 Langmead, B., Trapnell, C., Pop, M., and Salzberg, S.L. (2009). Ultrafast and memory-

1185 efficient alignment of short DNA sequences to the human genome. Genome Biol *10*, R25.

1186 Lettice, L.A., Heaney, S.J., Purdie, L.A., Li, L., de Beer, P., Oostra, B.A., Goode, D., Elgar,

1187 G., Hill, R.E., and de Graaff, E. (2003). A long-range Shh enhancer regulates expression in

1188 the developing limb and fin and is associated with preaxial polydactyly. Hum Mol Genet *12*,

1189 1725–1735.

1190 Li, H. (2011). A statistical framework for SNP calling, mutation discovery, association

1191 mapping and population genetical parameter estimation from sequencing data. Bioinformatics

1192 *27*, 2987–2993.

1193 Li, H. (2018). Minimap2: pairwise alignment for nucleotide sequences. Bioinformatics *34*,

1194 3094–3100.

1195 Li, H., Handsaker, B., Wysoker, A., Fennell, T., Ruan, J., Homer, N., Marth, G., Abecasis,

1196 G., Durbin, R., and Genome Project Data Processing, S. (2009). The Sequence

1197 Alignment/Map format and SAMtools. Bioinformatics *25*, 2078–2079.

1198 Liu, N., Hargreaves, V.V., Zhu, Q., Kurland, J.V., Hong, J., Kim, W., Sher, F., Macias-

37

1199 Trevino, C., Rogers, J.M., Kurita, R., et al. (2018). Direct Promoter Repression by BCL11A

1200 Controls the Fetal to Adult Hemoglobin Switch. Cell *173*, 430-442.e17.

1201 Lonfat, N., Montavon, T., Darbellay, F., Gitto, S., and Duboule, D. (2014). Convergent

1202 evolution of complex regulatory landscapes and pleiotropy at Hox loci. Science *346*, 1004–

1203 1006.

1204 Long, H.K., Prescott, S.L., and Wysocka, J. (2016). Ever-Changing Landscapes:

1205 Transcriptional Enhancers in Development and Evolution. Cell *167*, 1170–1187.

1206 Lopez-Delisle, L., Rabbani, L., Wolff, J., Bhardwaj, V., Backofen, R., Grüning, B., Ramírez,

1207 F., and Manke, T. (2021). pyGenomeTracks: reproducible plots for multivariate genomic

1208 datasets. Bioinformatics *37*, 422–423.

1209 Marinic, M., Aktas, T., Ruf, S., and Spitz, F. (2013). An integrated holo-enhancer unit

1210 defines tissue and gene specificity of the Fgf8 regulatory landscape. Dev. Cell *24*, 530–542.

1211 Martin, M. (2011). Cutadapt removes adapter sequences from high-throughput sequencing

1212 reads. EMBnet.Journal *17*.

1213 Montavon, T., Soshnikova, N., Mascrez, B., Joye, E., Thevenet, L., Splinter, E., de Laat, W.,

1214 Spitz, F., and Duboule, D. (2011). A regulatory archipelago controls Hox genes transcription

1215 in digits. Cell *147*, 1132–1145.

1216 Noordermeer, D., Leleu, M., Splinter, E., Rougemont, J., De Laat, W., and Duboule, D.

1217 (2011). The dynamic architecture of Hox gene clusters. Science *334*, 222–225.

1218 Nora, E.P., Lajoie, B.R., Schulz, E.G., Giorgetti, L., Okamoto, I., Servant, N., Piolot, T., van

1219 Berkum, N.L., Meisig, J., Sedat, J., et al. (2012). Spatial partitioning of the regulatory

1220 landscape of the X-inactivation centre. Nature *485*, 381–385.

1221 Osterwalder, M., Barozzi, I., Tissières, V., Fukuda-Yuzawa, Y., Mannion, B.J., Afzal, S.Y.,

1222 Lee, E.A., Zhu, Y., Plajzer-Frick, I., Pickle, C.S., et al. (2018). Enhancer redundancy

1223 provides phenotypic robustness in mammalian development. Nature *554*, 239–243.

1224 Oudelaar, A.M., Beagrie, R.A., Kassouf, M.T., and Higgs, D.R. (2021). The mouse alpha-

1225 globin cluster: a paradigm for studying genome regulation and organization. Curr. Opin.

1226 Genet. Dev. *67*, 18–24.

1227 Ramirez, F., Ryan, D.P., Gruning, B., Bhardwaj, V., Kilpert, F., Richter, A.S., Heyne, S.,

1228 Dundar, F., and Manke, T. (2016). deepTools2: a next generation web server for deep-

1229 sequencing data analysis. Nucleic Acids Res *44*, W160-5.

1230 Ramírez, F., Bhardwaj, V., Arrigoni, L., Lam, K.C., Grüning, B.A., Villaveces, J.,

1231 Habermann, B., Akhtar, A., and Manke, T. (2018). High-resolution TADs reveal DNA

1232 sequences underlying genome organization in flies. Nat. Commun. *9*, 189.

1233 Rodriguez-Carballo, E., Lopez-Delisle, L., Zhan, Y., Fabre, P.J., Beccari, L., El-Idrissi, I.,

1234 Huynh, T.H.N., Ozadam, H., Dekker, J., and Duboule, D. (2017). The HoxD cluster is a

38

1235 dynamic and resilient TAD boundary controlling the segregation of antagonistic regulatory

1236 landscapes. Genes Dev. *31*, 2264–2281.

1237 Rodríguez-Carballo, E., Lopez-Delisle, L., Willemin, A., Beccari, L., Gitto, S., Mascrez, B.,

1238 and Duboule, D. (2020). Chromatin topology and the timing of enhancer function at the

1239 *HoxD* locus. Proc. Natl. Acad. Sci. *117*, 31231–31241.

1240 Rouco, R., Bompadre, O., Rauseo, A., Fazio, O., Peraldi, R., Thorel, F., and Andrey, G.

1241 (2021). Cell-specific alterations in Pitx1 regulatory landscape activation caused by the loss of

1242 a single enhancer. Nat. Commun. *12*, 7235.

1243 Schaffner, W. (2015). Enhancers, enhancers – from their discovery to today's universe of

1244 transcription enhancers. Biol. Chem. *396*, 311–327.

1245 Schmidl, C., Rendeiro, A.F., Sheffield, N.C., and Bock, C. (2015). ChIPmentation: fast,

1246 robust, low-input ChIP-seq for histones and transcription factors. Nat Methods *12*, 963–965.

1247 Schuettengruber, B., Bourbon, H.-M., Di Croce, L., and Cavalli, G. (2017). Genome

1248 Regulation by Polycomb and Trithorax: 70 Years and Counting. Cell *171*, 34–57.

1249 Sexton, T., Yaffe, E., Kenigsberg, E., Bantignies, F., Leblanc, B., Hoichman, M., Parrinello,

1250 H., Tanay, A., and Cavalli, G. (2012). Three-dimensional folding and functional organization

1251 principles of the Drosophila genome. Cell *148*, 458–472.

1252 Shapiro, M.D., Marks, M.E., Peichel, C.L., Blackman, B.K., Nereng, K.S., Jonsson, B.,

1253 Schluter, D., and Kingsley, D.M. (2004). Genetic and developmental basis of evolutionary

1254 pelvic reduction in threespine sticklebacks. Nature *428*, 717–723.

1255 Sheth, R., Barozzi, I., Langlais, D., Osterwalder, M., Nemec, S., Carlson, H.L., Stadler, H.S.,

1256 Visel, A., Drouin, J., and Kmita, M. (2016). Distal Limb Patterning Requires Modulation of

1257 cis-Regulatory Activities by HOX13. Cell Rep *17*, 2913–2926.

1258 Skene, P.J., Henikoff, J.G., and Henikoff, S. (2018). Targeted in situ genome-wide profiling

1259 with high efficiency for low cell numbers. Nat. Protoc. *13*, 1006–1019.

1260 Spitz, F., Gonzalez, F., and Duboule, D. (2003). A global control region defines a

1261 chromosomal regulatory landscape containing the HoxD cluster. Cell *113*, 405–417.

1262 Tarchini, B., and Duboule, D. (2006). Control of Hoxd genes' collinearity during early limb

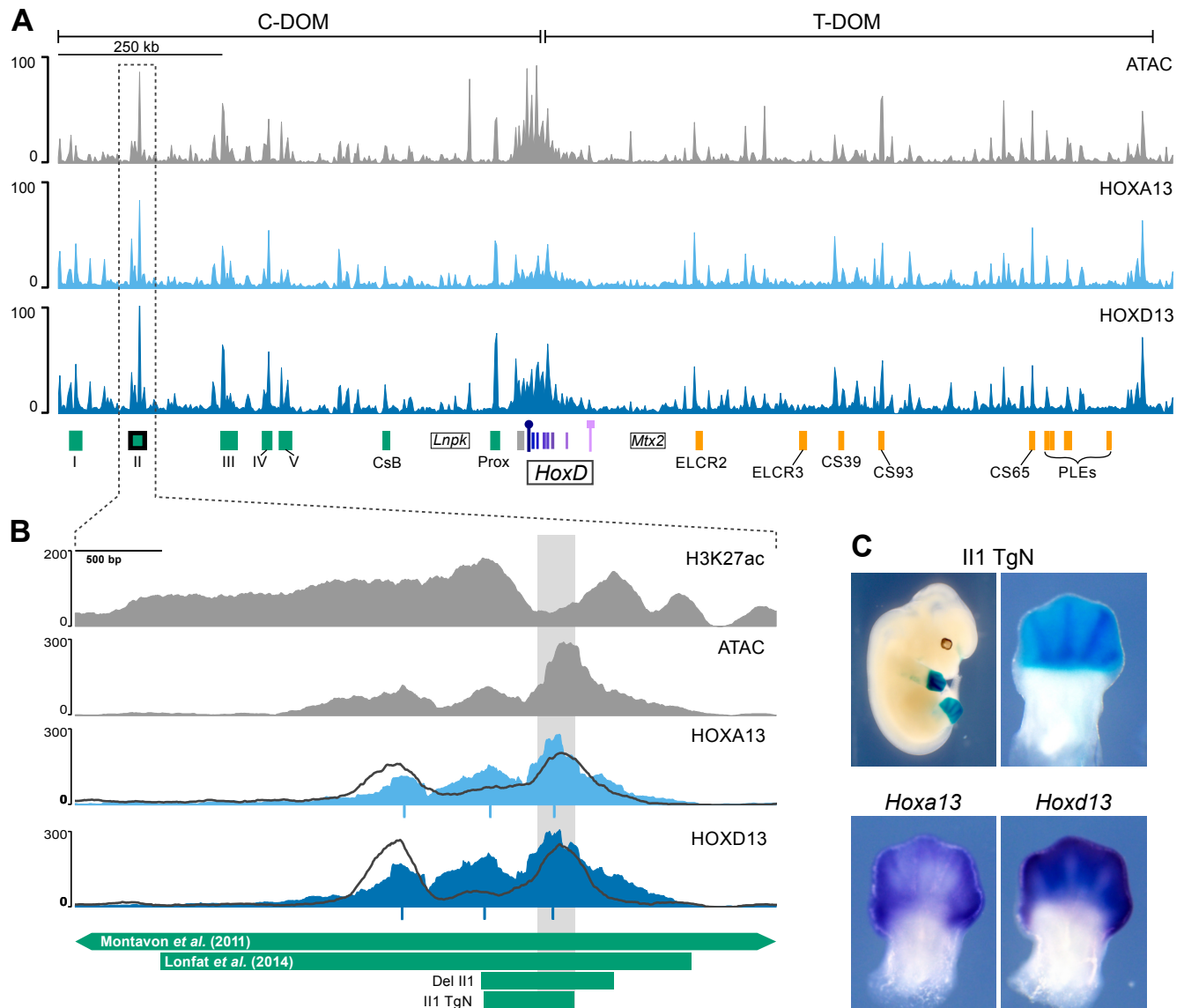1263 development. Dev Cell *10*, 93–103.

1264 Vieux-Rochas, M., Fabre, P.J., Leleu, M., Duboule, D., and Noordermeer, D. (2015).

1265 Clustering of mammalian Hox genes with other H3K27me3 targets within an active nuclear

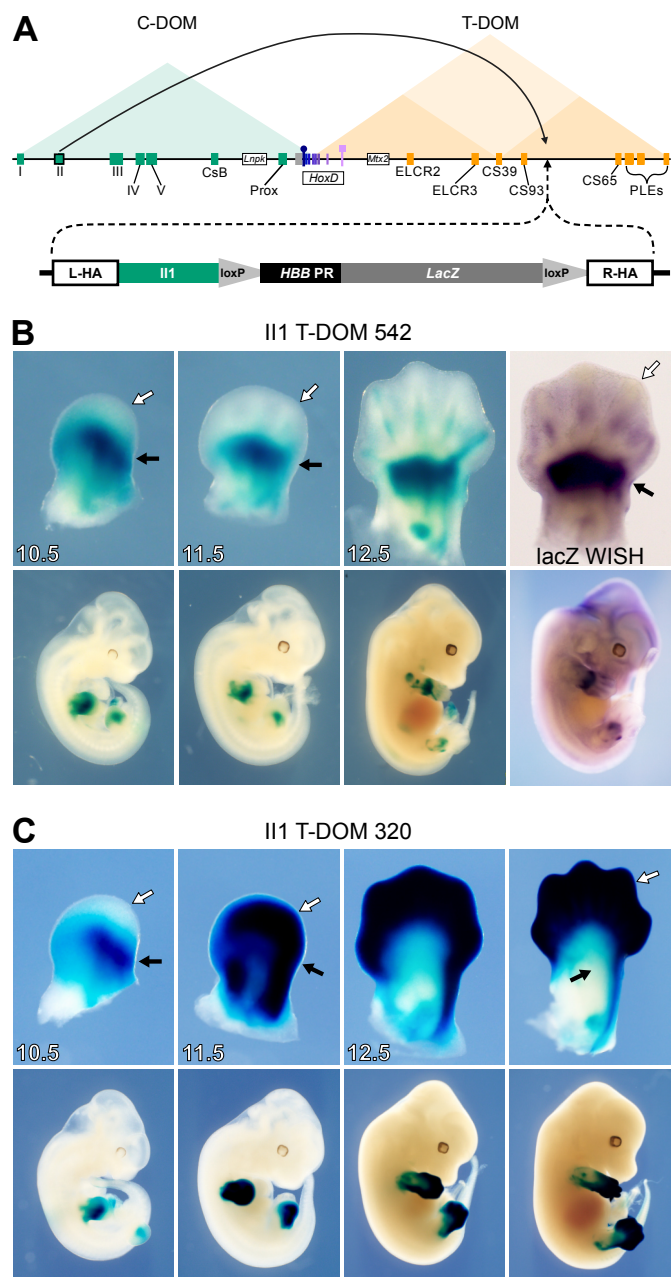1266 domain. Proc Natl Acad Sci U A *112*, 4672–4677.

1267 Wolff, J., Rabbani, L., Gilsbach, R., Richard, G., Manke, T., Backofen, R., and Grüning,

1268 B.A. (2020). Galaxy HiCExplorer 3: a web server for reproducible Hi-C, capture Hi-C and

1269 single-cell Hi-C data analysis, quality control and visualization. Nucleic Acids Res. *48*,
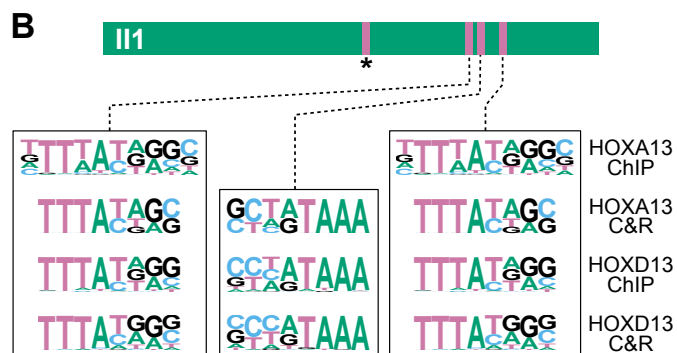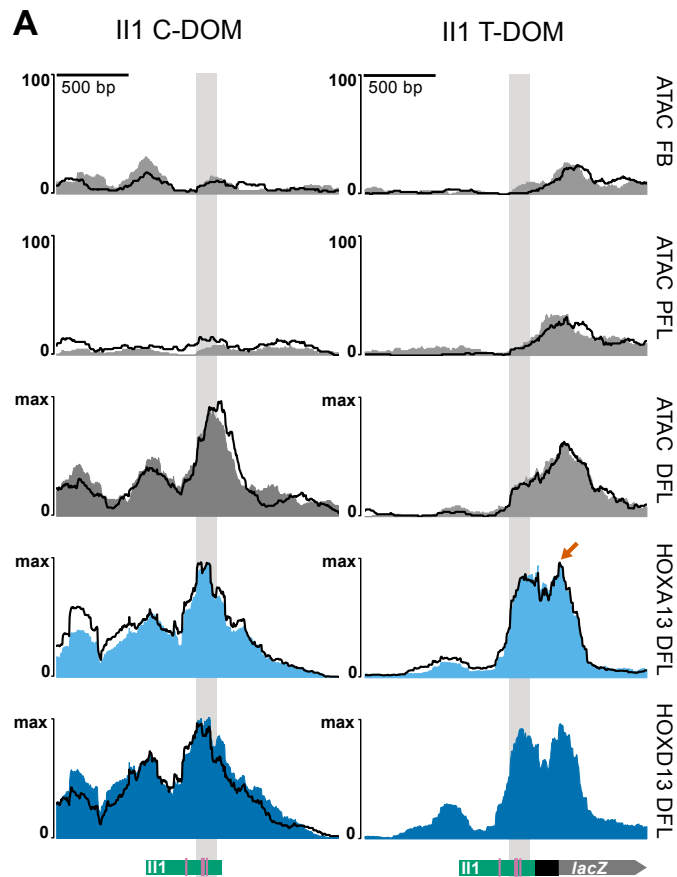
1270 W177–W184.

39

1271   Wolff, P., Weinhofer, I., Seguin, J., Roszak, P., Beisel, C., Donoghue, M.T., Spillane, C.,

1272   Nordborg, M., Rehmsmeier, M., and Kohler, C. (2011). High-resolution analysis of parent-

1273   of-origin allelic expression in the Arabidopsis Endosperm. PLoS Genet *7*, e1002126.

1274   Woltering, J.M., and Duboule, D. (2010). The origin of digits: expression patterns versus

1275   regulatory mechanisms. Dev Cell *18*, 526–532.

1276   Woltering, J.M., Vonk, F.J., Muller, H., Bardine, N., Tuduce, I.L., de Bakker, M.A.,

1277   Knochel, W., Sirbu, I.O., Durston, A.J., and Richardson, M.K. (2009). Axial patterning in

1278   snakes and caecilians: evidence for an alternative interpretation of the Hox code. Dev Biol

1279   *332*, 82–89.

1280   Woltering, J.M., Noordermeer, D., Leleu, M., and Duboule, D. (2014). Conservation and

1281   divergence of regulatory strategies at Hox Loci and the origin of tetrapod digits. PLoS Biol

1282   *12*, e1001773.

1283   Yakushiji-Kaminatsui, N., Lopez-Delisle, L., Bolt, C.C., Andrey, G., Beccari, L., and

1284   Duboule, D. (2018). Similarities and differences in the regulation of HoxD genes during

1285   chick and mouse limb development. PLoS Biol. *16*, e3000004.

1286   Zakany, J., and Duboule, D. (2007). The role of Hox genes during vertebrate limb

1287   development. Curr. Opin. Genet. Dev. *17*, 359–366.

1288   Zhang, Y., Liu, T., Meyer, C.A., Eeckhoute, J., Johnson, D.S., Bernstein, B.E., Nusbaum, C.,

1289   Myers, R.M., Brown, M., Li, W., et al. (2008). Model-based analysis of ChIP-Seq (MACS).
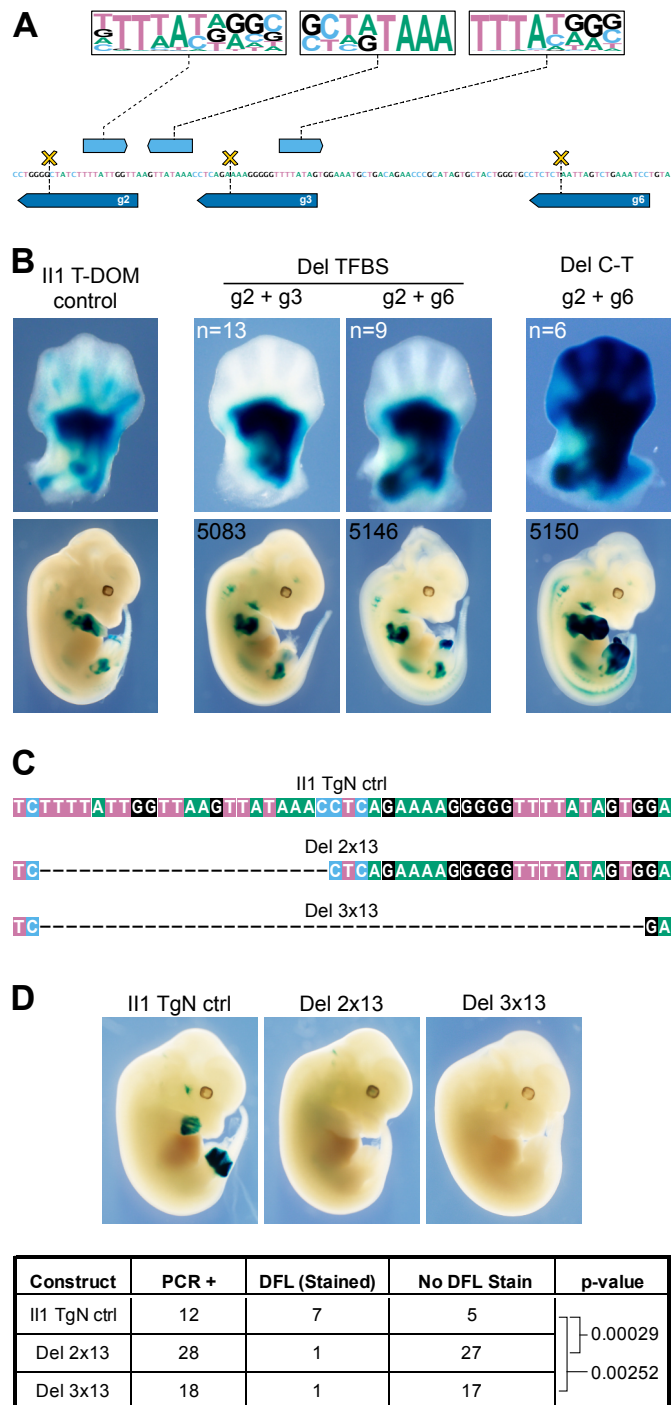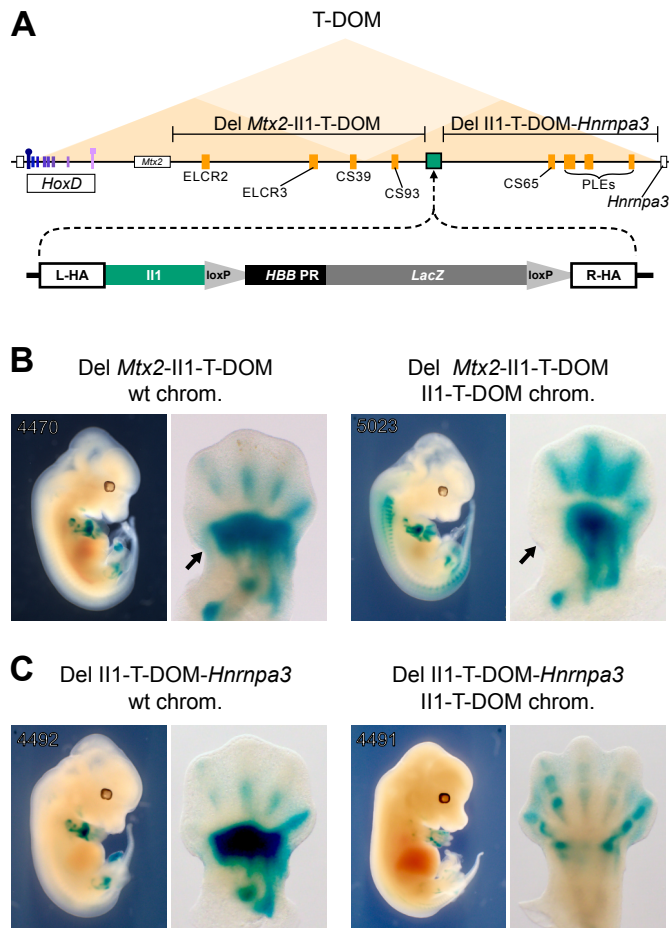
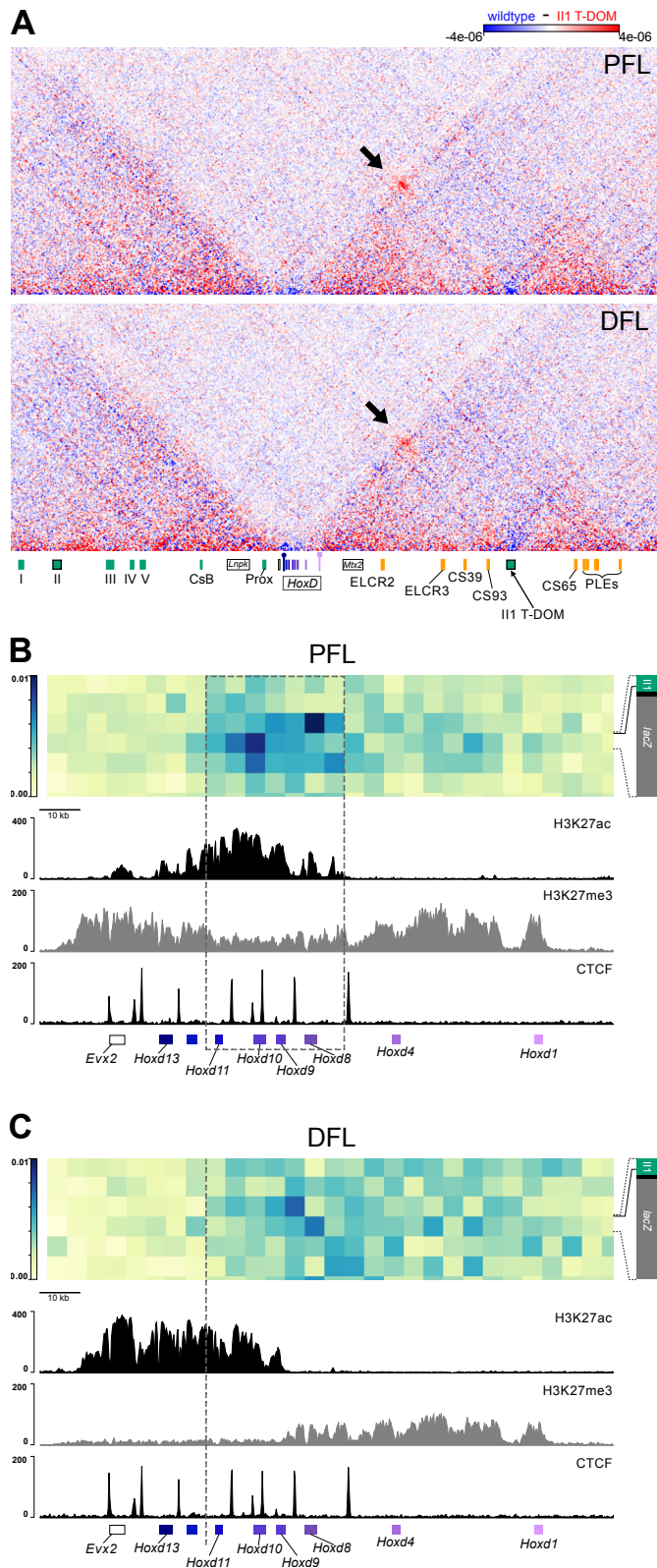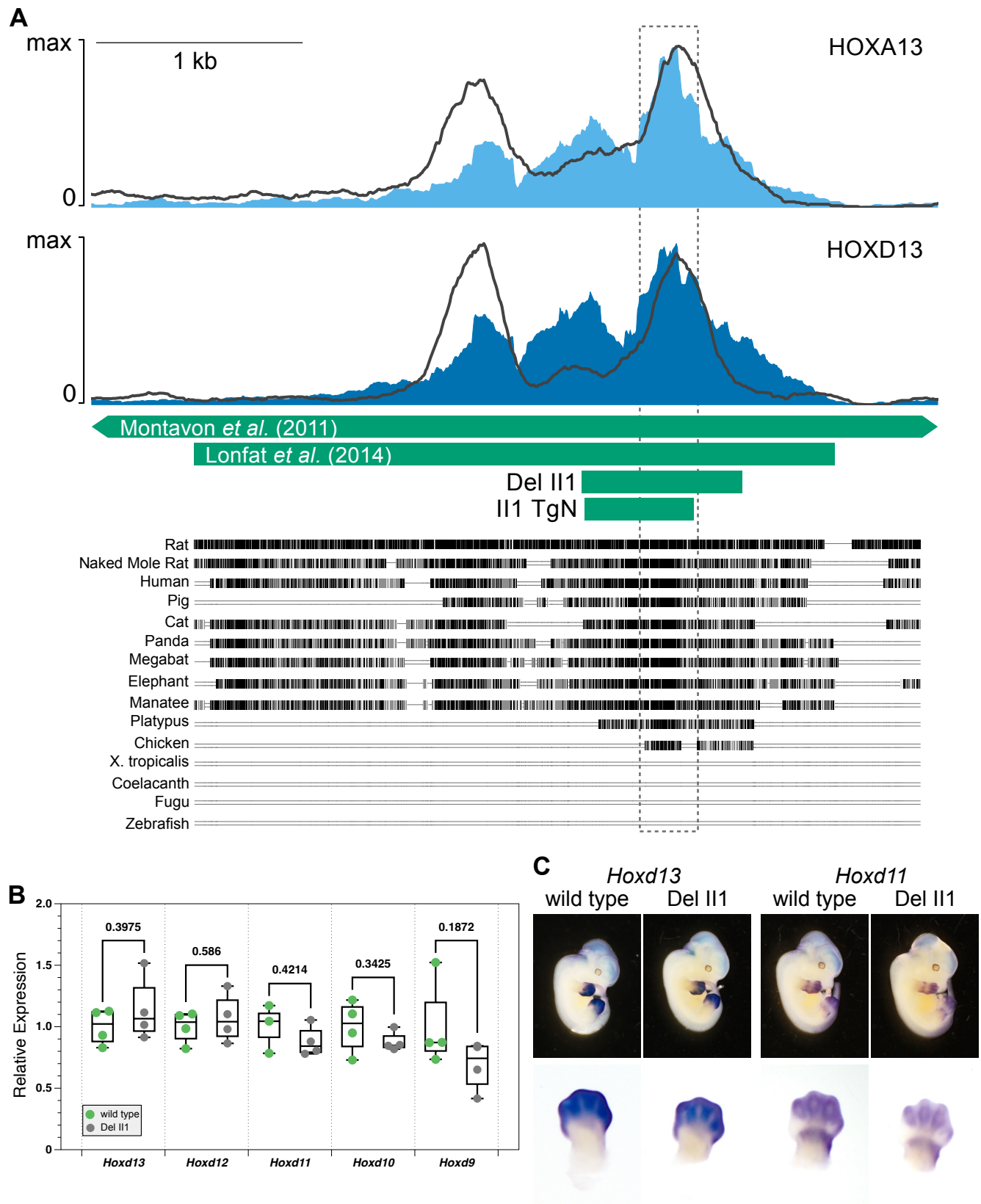1290   Genome Biol *9*, R137.

1291

1292

Bolt 2021, Il1TDOM Figure 1

Bolt 2021, Il1TDOM Figure 2

Bolt 2021, Il1TDOM Figure 3

Bolt 2021, Il1TDOM Figure 4

Bolt 2021, II1TDOM Figure 5

Bolt 2021, II1TDOM Figure 6

Bolt 2021, Il1TDOM Figure S1

Bolt 2021, Il1TDOM Figure S2

Bolt 2021, Il1TDOM Figure S4-1

Il1 TgN ctrl

15.07.20 w04 cb12 01   15.07.20 w03 cb09 04

15.07.20 w03 cb09 03   15.07.20 w03 cb09 02

15.07.20 w03 cb09 01   14.07.20 w05 cb04 01

14.07.20 w04 cb03 01   14.07.20 w03 cb02 01

14.07.20 w01 cb01 01

Del 2x13

21.10.20 w02 cb30 01   06.10.20 w01 CB17 01

20.10.20 w05 cb24 01   20.10.20 w02 cb26 01

06.10.20 w03 cb19 01   06.10.20 w04 cb21 01

06.10.20 w01 CB17 05   06.10.20 w01 CB17 04

06.10.20 w01 CB17 03   06.10.20 w01 CB17 02

Del 3x13

15.07.20 w06 cb15 01   15.07.20 w05 cb14 01

14.07.20 w11 cb07 01   15.07.20 w01 cb08 01

Bolt 2021, Il1TDOM Figure S4-2

A Del 3x13 T-DOM

B *HBB:lacZ* T-DOM
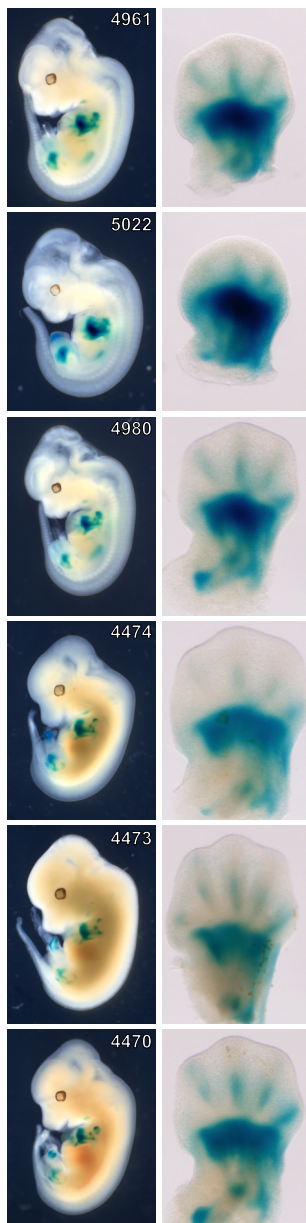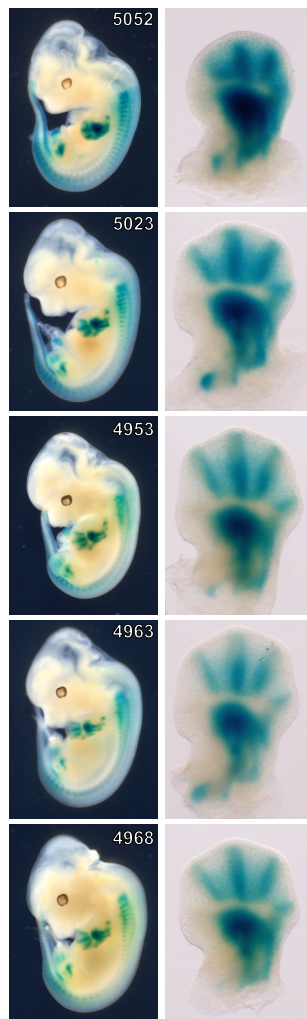

Bolt 2021, Il1TDOM Figure S4-3
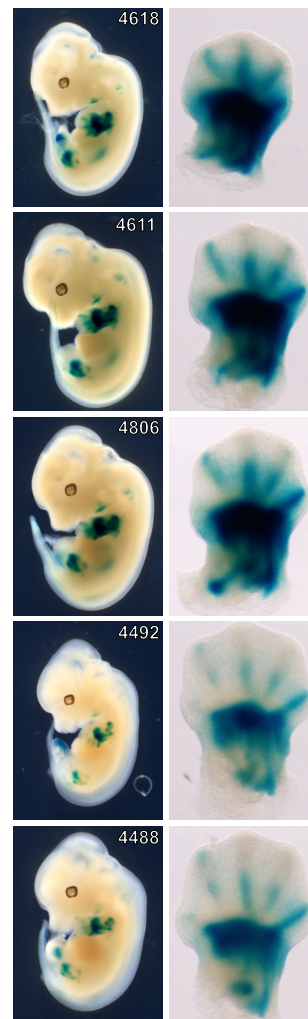
A

Del *Mtx2*-Il1-T-DOM
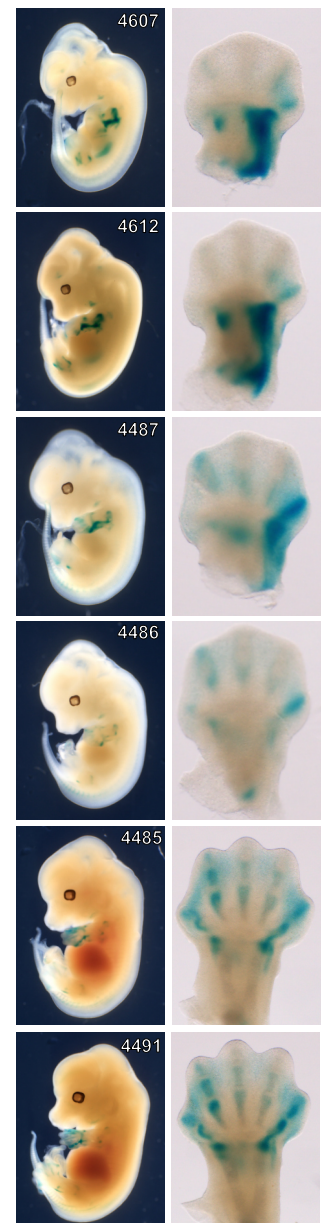wt chrom.

Del *Mtx2*-Il1-T-DOM
Il1-T-DOM chrom.

B

Del Il1-T-DOM-*Hnrnpa3*
wt chrom.

Del Il1-T-DOM-*Hnrnpa3*
Il1-T-DOM chrom.

Bolt 2021, Il1TDOM Figure S5

A

Bolt 2021, II1TDOM Figure S6